HYDRODYNAMIC MODELING OF THE TIDAL PRISM IN THE PONTCHARTRAIN BASIN

Draft Final Report

Project Team Members

J. Alex McCorquodale [1], Ioannis Georgiou [2], Angel Gabriel Retana[3], Donald Barbe [1], Martin J. Guillot[4]

[1] Professor, Dept. of Civil and Environmental Engineering, University of New Orleans, New Orleans LA 70148
[2] Assistant Professor, Pontchartrain Institute for Environmental Sciences and Department of Earth and Environmental Sciences, University of New Orleans, New Orleans LA 70148
[3] PhD Candidate, Dept. of Civil and Environmental Engineering, University of New Orleans, New Orleans LA 70148
[4] Associate Professor, Dept. of Mechanical Engineering, University of New Orleans, New Orleans LA 70148

June 2007

EXECUTIVE SUMMARY

The focus of this study was the response of tides in Lake Pontchartrain to changes in the tidal passes and navigation waterways.

The effects of changes in the passes and the waterways were investigated using the unstructured 3-D Finite Volume Coastal Ocean Model, FVCOM. Model runs simulated spring discharge conditions with representative tides, tributary flows and extratropical storms surges. The spring period corresponds to the time when the Mississippi River is at it maximum annual stage and the period when an opening of the Bonnet Carré Spillway is most likely to occur. The effects of structures on tides and stages in Lake Pontchartrain during a Bonnet Carré Spillway opening was also simulated using the 1997 Spillway Hydrograph.

The following Structural Options were considered:

- Existing passes and navigational waterways
- Modified navigational waterways with shallow draft openings
- Existing passes with flood gate structures and modified navigational waterways with shallow draft openings

The structural options were combined with several hydraulic boundary conditions:

- Normal diurnal tides
- Normal diurnal tides plus an extratropical storm surge
- Normal tides plus the 1997 Bonnet Carré Spillway hydrograph
- Normal diurnal tides plus an extratropical storm surge plus the 1997 Bonnet Carré Spillway hydrograph.

The structure opening for the Rigolets was varied from approximately 800 ft to 1975 ft with a sill at -30 ft. The structure in the Chef Menteur Pass was varied from 700 to 1000 ft in width with a sill at -30 ft. The recommended structural option was selected based on an assessment of no significant impact on the tidal prism in Lake Pontchartrain. Other considerations included minimum effect on the stage in Lake Pontchartrain during Bonnet Carré Spillway operation and during extratropical storm surges.

It was found that the original 1985 structures had a significant attenuating effect on the tidal prism in Lake Pontchartrain. In addition, the local velocities exceeded 25 % of the maximum velocities in the Passes without structures. The FVCOM and ECOMSED modeling showed that the Rigolets flood control structure should have a clear opening of 1700 ft and the Chef structure should have a clear opening of 700 ft to keep the reduction in the tidal prism equal or less than 5 % compared to the existing conditions with the modified waterways. The introduction of shallow draft openings at the MRGO, the ICWW and the IHNC resulted in a 3 % reduction in the tidal prism in Lake Pontchartrain. The combination of the 1700 ft wide structure in the Rigolets and the 750 ft wide structure in the Chef Pass along with the shallow water constrictions in the navigational waterways caused an upward shift in the normal stage in Lake Pontchartrain of approximately 2 mm (less than 1/10 inch) for normal spring tributary flows and normal tides. The maximum increase in the local velocity during normal tides for the above structures is less

than 25 % and is restricted to approximately 2 channel widths east and west of the Rigolets structure and less for the Chef structure. The model showed that 405 of the open at the structure would have velocities less than the maximum without the structure. The proposed structure widths and the shallow draft changes to the waterway will result in a minor increase in the Lake Pontchartrain stage during a Bonnet Carré Spillway event similar to the 1997 opening. Similarly, the combination of the proposed structural changes with a combination of a Bonnet Carré Operation and an extratropical storm surge does not significantly change the maximum stage in Lake Pontchartrain.

Contents

List of Figures

List of Tables

Introduction and Background

The Lake Pontchartrain Basin is located north of New Orleans in southeastern Louisiana, USA, as shown in Figure 1. This complex estuarine ecosystem consists of three main water bodies that are interconnected by narrow passes, numerous freshwater rivers, as well as shipping canals, outfalls, and surrounding marshes and wetlands. The basin has formed in a shallow depression lying between the alluvial ridge of the Mississippi River to the west and the sloping uplands to the north. Lake Maurepas is located to the west, and is predominantly freshwater, receiving water from the Blind, Amite, and Tickfaw Rivers. Lake Maurepas is connected to Lake Pontchartrain, through a narrow passage called Pass Manchac. Lake Borgne is an estuary located east of Lake Pontchartrain; this estuary has an open boundary with an embayment of the Gulf of Mexico and is connected to Lake Pontchartrain through two natural tidal passes, Chef Menteur Pass and The Rigolets. In addition, the Inner Harbor Navigation Canal (IHNC), which enters into the southeastern corner of Lake Pontchartrain, serves as a third tidal pass. The Mississippi River is separated from the Lake Pontchartrain Basin by levees, but is connected at two locations, the Bonnet Carré Spillway and through a lock at the IHNC. The spillway is a component of the Mississippi River and Tributaries Flood 2 Control project, designed to operate as a relief valve during potential flooding conditions at New Orleans. Table 1 summarizes some of the important data on the physical and demographic characteristics of the Lake Pontchartrain System.

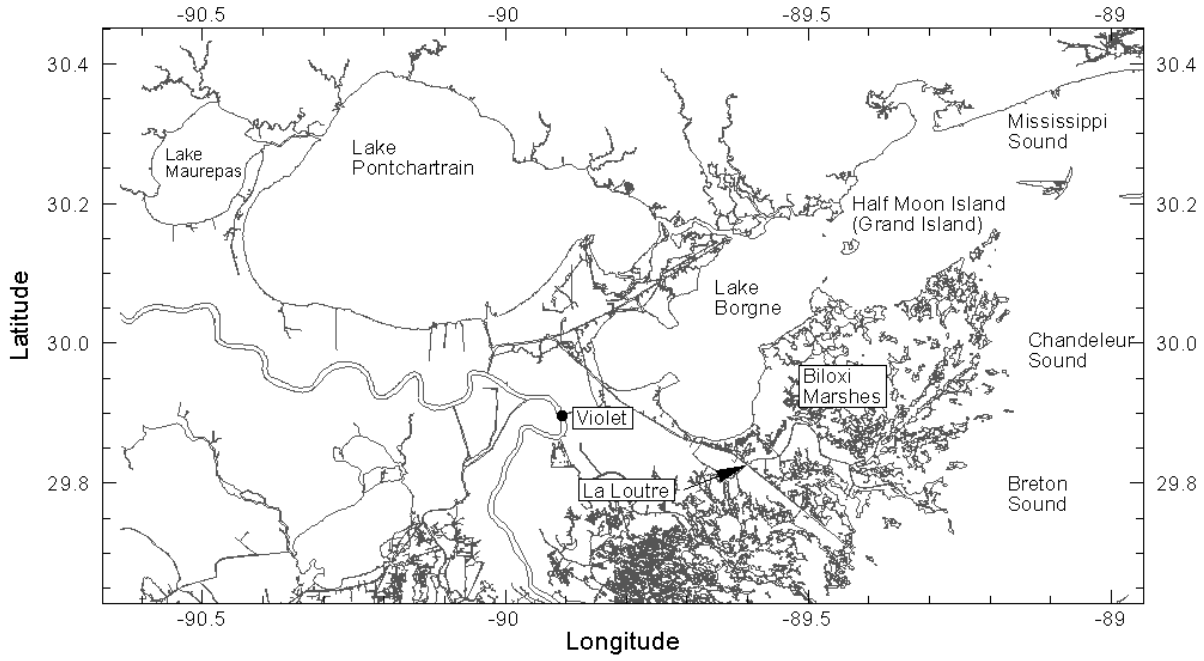

Figure 1 Map of the Pontchartrain Basin

Table 1 Basin Physical and Demographic Data

Basin mean annual rainfall	1.47 m
Basin population	1.5 million people
Lake Pontchartrain average depth	3.7 m
Lake Pontchartrain classification	brackish
Lake Pontchartrain north-south axis	40.2 km
Lake Pontchartrain east-west axis	64.4 km
Lake Pontchartrain surface area	1630 km^2
Lake Pontchartrain uses	fishing, crabbing, swimming, boating
Lake Pontchartrain tides	diurnal; mean range of 0.11 m
Lake Pontchartrain tidal prism	$1.6x10^8$ m^3
Lake Pontchartrain water column	generally well mixed
Lake Pontchartrain stratification	stronger at certain times near the IHNC
The Rigolets Pass total length average depth cross-sectional area	 14.5 km 8 m 7500 m^2
Chef Menteur Pass total length average depth cross-sectional area	 11.3 km 13 m 2422 m^2
IHNC-MRGO total length average depth cross-sectional area	 30 km 7.5 m 1125 m^2
Pass Manchac total length average depth cross-sectional area	 15 km 8 m 2924 m^2
Lake Maurepas surface area	233 km^2
Lake Maurepas average depth	3.0 m
Lake Borgne surface area	550 km^2
Lake Borgne average depth	2.7 m

* After Haralampides, 2000

Study Objectives

The main objective of this study is to determine the hydrodynamic impacts of proposed structural changes to the tidal passes and the navigational waterways by the use of hydrodynamic models. In addition, mathematical modeling will be used to determine the dimensions of flood control structures in the Rigolets and Chef Menteur Passes that would have minimal impact on the tidal prism of Lake Pontchartrain under normal conditions when the gates are open.

Study Scenarios

Table 2 shows the structural and boundary condition options that were considered in this study. Detailed high resolution 3-D modeling was completed for peak ebb and flood flows at the Rigolets and Chef structures. The proposed locations of the structures and the shallow draft constrictions in the navigational waterways are shown in Figure 2.

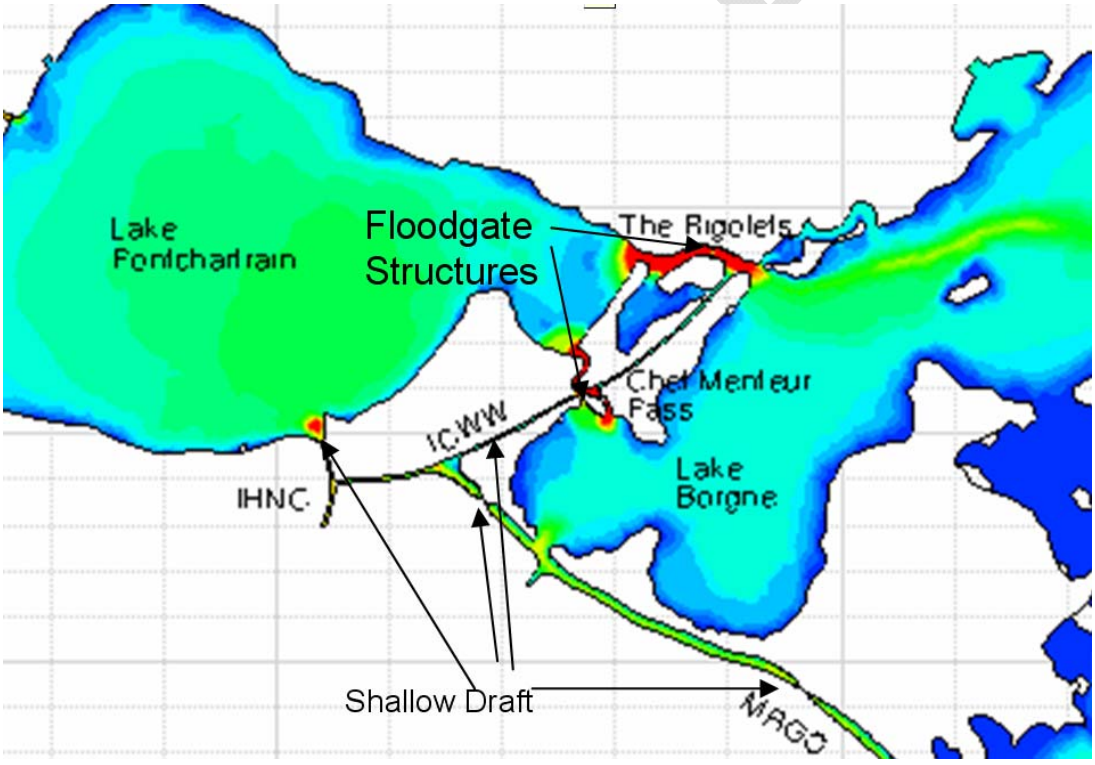

Figure 2 Proposed locations of structures and channel modifications

Table 2 Structural and Boundary Scenarios

FVCOM

Runs

First set of runs	Clear opening **	Clear opening				
Title	Rigolets	Chef	MRGO	ICWW	IHNC	Condition
1	Existing	existing	existing	existing	Existing	Normal
4	Existing	existing	existing	existing	Existing	Extratropical
2	Existing	existing	existing	existing	Existing	Bonnet Carré open, Normal
3	Existing	existing	existing	existing	Existing	Bonnet Carré open, Extratropical
	1500 open	700 open	Shallow at Bayou La Loutre and Bayou Bienvenu	Blocked, Lake St. Catherine blocked	Shallow	Bonnet Carré open, Extratropical
6a	1500 open	700 open	Shallow at Bayou La Loutre and Bayou Bienvenu	Blocked, Lake St. Catherine blocked	Shallow	Normal
	1500 open	700 open	Shallow at Bayou La Loutre and Bayou Bienvenu	Blocked, Lake St. Catherine blocked	Shallow	Extratropical
Second set of runs						
Title	Rigolets	Chef	MRGO	ICWW	IHNC	Condition
5	Existing	existing	Shallow at Bayou La Loutre, Bayou Bienvenu, and Bayou Daytoe	existing	Shallow	Normal
8c	Existing	existing	Shallow at Bayou La Loutre, Bayou Bienvenu, and Bayou Daytoe	existing	Shallow	Bonnet Carré open, Normal
6b	1700 open	700 open	Shallow at Bayou La Loutre, Bayou Bienvenu, and Bayou Daytoe	Blocked, Lake St. Catherine blocked	Shallow	Normal
8b	1700 open	700 open	Shallow at Bayou La Loutre, Bayou Bienvenu, and Bayou Daytoe	Blocked, Lake St. Catherine blocked	Shallow	Bonnet Carré open, Normal
9b	1700 open	700 open	Shallow at Bayou La Loutre, Bayou Bienvenu, and Bayou Daytoe	Blocked, Lake St. Catherine blocked	Shallow	Bonnet Carré open, Extratropical
Third run						
Title	Rigolets	Chef	MRGO	ICWW	IHNC	Condition
6c	1700 open	600 open	Shallow at Bayou La Loutre, Bayou Bienvenu, and Bayou Daytoe	Blocked, Lake St. Catherine blocked	Shallow	Normal

**Add approximately 15% for total width of structure.

Methodology and Technical Approach

Hydrodynamic modeling in the Pontchartrain estuary was performed using the Finite Volume Coastal Ocean Model (FVCOM) to establish baseline (present) conditions. Once baseline conditions were established and the model calibrated, various structural options were simulated to assess their impact on the tidal prism in Lake Pontchartrain. The model was used to simulate water levels and velocity distributions resulting from tidal variations with and without structural changes to the passes and the navigational waterways. Simulations were repeated to investigate the hydrodynamic response of the system for normal tides and special conditions such as the presence of an extratropical storm or the Bonnet Carré Spillway open. The resulting elevation and velocity changes were compared to estimate the effect on the system and propose alternatives due to the inclusion of these structures under different conditions.

The ECOMSED Model (HydroQual) was used to obtain better resolution of the currents near the structures in the Rigolets and Chef Menteur Passes. The velocity fields were examined to determine maximum velocities, longitudinal and lateral extent of the elevated velocities, recirculation zones and any tendency for the flow to attach to the channel banks. This model also provided head loss characteristics for the different structural options.

Numerical Modeling

System Modeling (FVCOM)

Model Description

FVCOM is a prognostic, unstructured-grid, finite-volume, free-surface, 3-D primitive equation coastal ocean circulation model developed by the University of Massachusetts at Dartmouth and the Woods Hole Oceanographic Institute (UMASSD-WHOI) joint efforts. The model consists of momentum, continuity, temperature, salinity and density equations and is closed physically and mathematically using turbulence closure sub-models (Burchard, 2002, Mellor and Yamada, 1984). The horizontal grid is composed of unstructured triangular cells and the irregular bottom is presented using generalized terrain-following coordinates or otherwise known as sigma coordinates. FVCOM is solved numerically by a second-order accurate discrete flux calculation in the integral form of the following governing equations over an unstructured triangular grid.

$$\frac{\partial u}{\partial t}+u\frac{\partial u}{\partial x}+v\frac{\partial u}{\partial y}+w\frac{\partial u}{\partial z}-fv=-\frac{1}{\rho_o}\frac{\partial P}{\partial x}+\frac{\partial}{\partial z}\left(K_m\frac{\partial u}{\partial z}\right)+F_u \quad (1)$$

$$\frac{\partial v}{\partial t}+u\frac{\partial v}{\partial x}+v\frac{\partial v}{\partial y}+w\frac{\partial v}{\partial z}-fu=-\frac{1}{\rho_o}\frac{\partial P}{\partial y}+\frac{\partial}{\partial z}\left(K_m\frac{\partial v}{\partial z}\right)+F_v \quad (2)$$

$$\frac{\partial P}{\partial z}=-\rho g \quad (3)$$

$$\frac{\partial u}{\partial x}+\frac{\partial v}{\partial y}+\frac{\partial w}{\partial z}=0 \quad (4)$$

$$\frac{\partial S}{\partial t} + u\frac{\partial S}{\partial x} + v\frac{\partial S}{\partial y} + w\frac{\partial S}{\partial z} = \frac{\partial}{\partial z}\left(K_h \frac{\partial S}{\partial z}\right) + F_S \qquad (5)$$

where x, y, and z are the east, north, and vertical axes in the Cartesian coordinate system; u, v and w are the x, y, and z velocity components; P is the pressure; f is the Coriolis parameter; g is the gravitational acceleration; S is the salinity; K_m is the vertical eddy viscosity coefficient; K_h is the thermal vertical eddy diffusion coefficient, and F_u, F_v, and F_S represent the horizontal momentum and salt diffusion term respectively.

The computation of the vertical eddy viscosity and thermal diffusion coefficient are based on the Mellor and Yamada (1982) level 2.5 (MY-2.5) *k-l* turbulent closure model where *k* is the turbulent kinetic energy and *l* is the turbulent macroscale. The horizontal diffusion coefficient is computed using the Smagorinski eddy parameterization method (Smagorinsky, 1963), which varies with the model resolution and the gradient of the horizontal velocities. The General Ocean Turbulent Model (GOTM) developed by (Burchard, 2002) has been added to FVCOM to provide optional vertical turbulent closure schemes.

This approach combines the best features of finite-element methods (grid flexibility) and finite-difference methods (numerical efficiency and code simplicity) and provides a much better numerical representation of both local and global momentum, mass, salt, heat, and tracer conservation. FVCOM runs on a UNIX or LINUX platform, and is written with Fortran 90 with MPI parallelization. The code runs efficiently on single and multi-processor machines. The model structure and available modules and sub-models are shown in Figure 3.

For a more detailed description and for information regarding the model's governing equations, model parameterization, and details on turbulence, numerical methods, and the solution of the governing equations, the reader is directed to Chen et al, 2003.

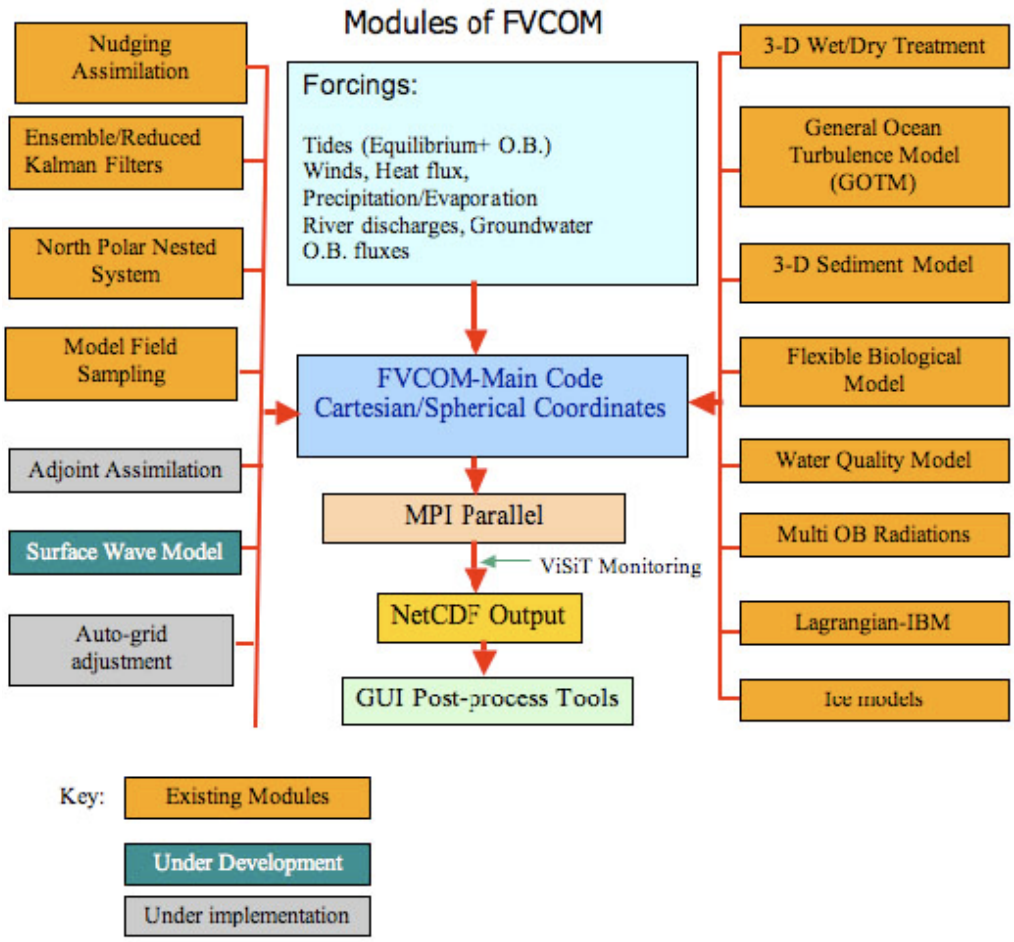

Figure 3 Model structure of FVCOM and available modules/sub-models (Chen et al, 2006)

Model Setup

The model was setup for an area of the Pontchartrain Basin that includes Lakes Maurepas, Pontchartrain and Borgne, the Biloxi Marshes, and the Mississippi, Breton and Chandeleur Sounds. The computational domain consists of 8904 computational nodes and 15523 elements (Figure 4). Grid resolution varies from 800 m near the open boundary to 30 m in the tidal passes; for the scenarios where the navigation channels were constricted, the local element size was 30-75 meters. The model consists of 3 vertical layers at this stage, although versions of the grid with 11 layers were tested. Simulation times for the model were 5 days per 30 day run on a single CPU.

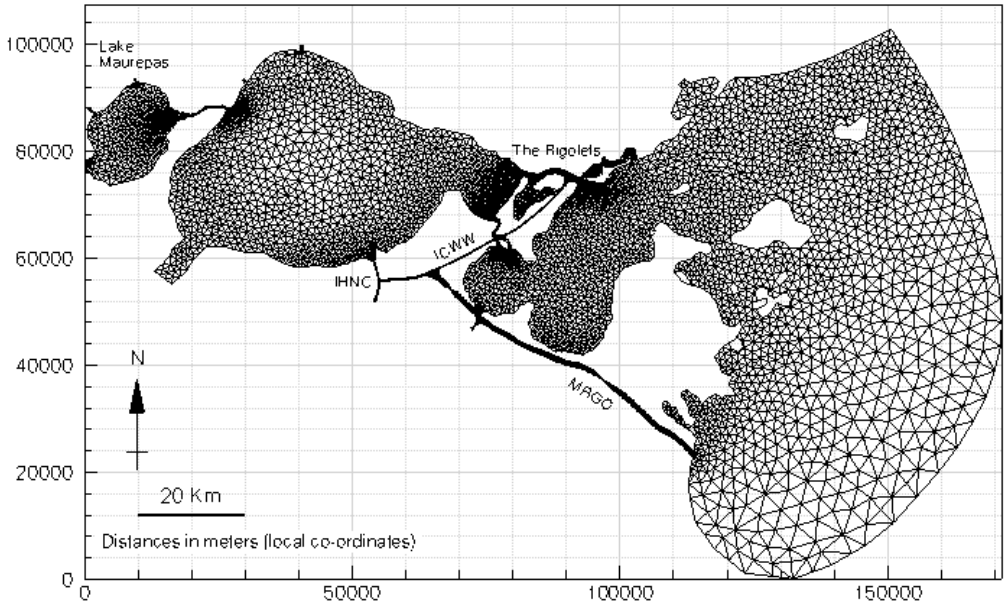

Figure 4 FVCOM - Model computational domain.

Initial Conditions

The model bathymetry for the model was obtained from a combination of sources; National Oceanic and Atmospheric Administration (NOAA) National Ocean Service (NOS) hydrographic surveys, and supplements from the US Geological Survey in 1996. Additional data in Breton and Chandeleur Sound were obtained from the Advance Circulation Model grid ADCIRC version SL15v3. The model bathymetry is shown in Figure 5.

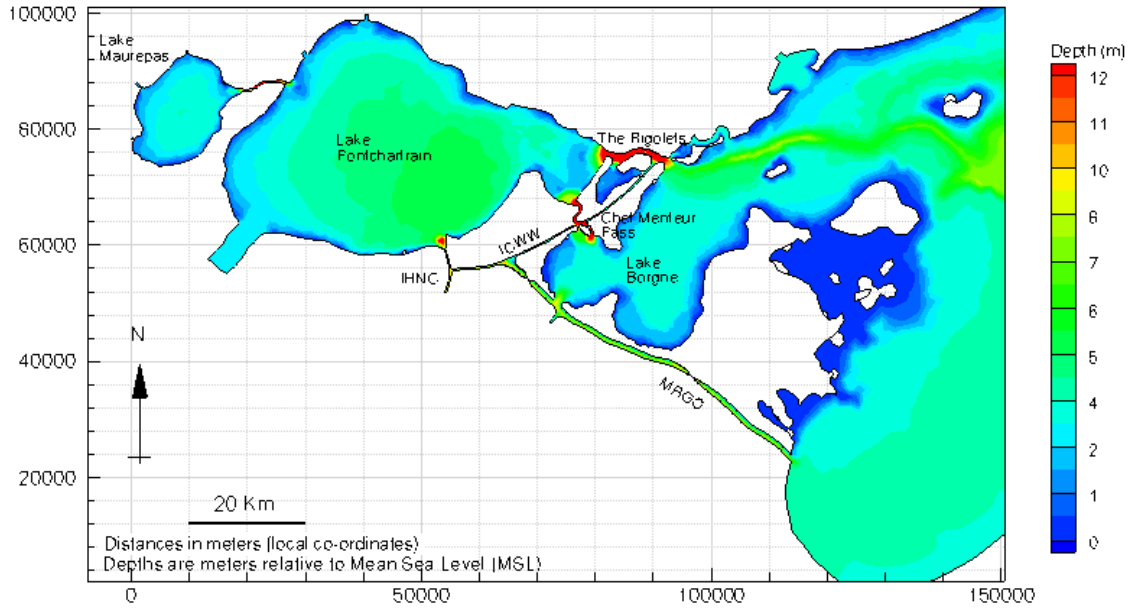

Figure 5 Model Bathymetry Relative to Mean Sea Level.

Salinity was included in the FVCOM simulations without calibration. The runs were not sufficiently long to assess the impacts of the proposed changes on the salinity in the system. Initial salinity conditions were generated using datasets collected from 1997 through 2002 by Haralampides (2000), Georgiou (2002) and Dr. Martin O'Connell from 2003 through 2006 (pers. comm.). These datasets were used to generate average conditions for a normal year. In areas with little or no data interpolation methods were used to fill the gaps, while maintaining a realistic estuarine salinity gradient. Figure 6 shows the distribution of salinities that were used as the initial condition for all simulations.

For all simulations, initial elevation was set to zero (relative to mean sea level – MSL). The model started each simulation from rest (still water surface) and the spin-up times for all boundary conditions (tributary flows and tidal elevations at open boundaries) were of the order of hours.

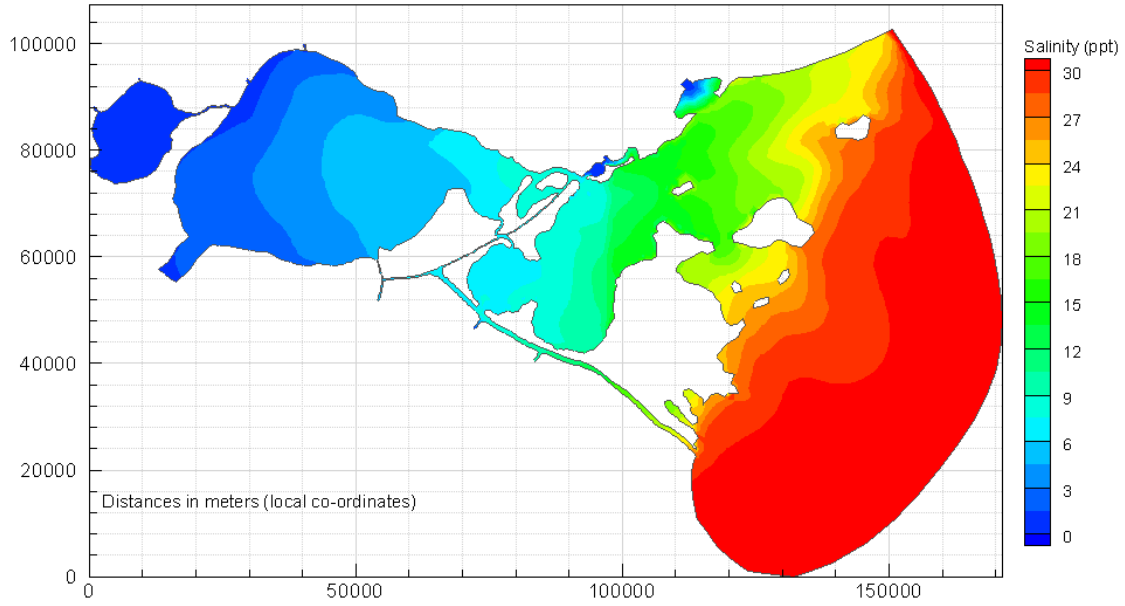

Figure 6 Initial condition for salinity used in the model. The salinity gradient represents average conditions for the last 10 years.

Boundary Conditions

Tidal and salinity data were collected from a number of stations for hourly water level and salinity, wind speed and direction, temperature and other parameters. Tidal boundaries for calibration were obtained from Dr. Ray Chapman at the Engineering Research and Development Center (ERDC) at the locations shown in Figure 7. Tides in the area are mainly diurnal with varying ranges throughout the estuary. The tidal conditions at the open boundary were the same for all simulations; however, additional simulations were completed with an extratropical storm surge superimposed on the normal tides and with the 1997 Bonnet Carré hydrograph. The normal diurnal tidal boundary condition is shown in Figure 8. The superposition of a storm surge on the normal tide is presented in Figure 9. The 1997 Bonnet Carré hydrograph is given in Figure 10. Figure 11 shows the tributary flows that were used in the model.

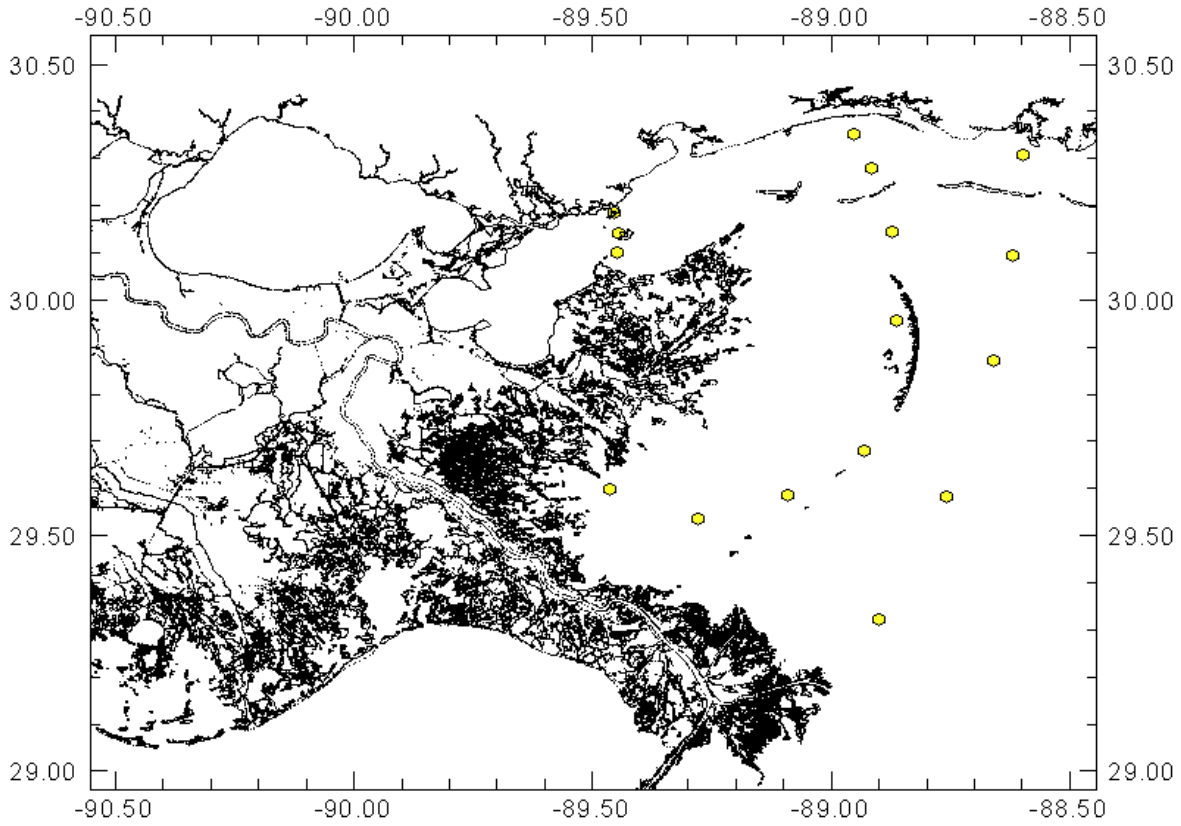

Figure 7 Locations of ADCIRC generated tides for hindcast calibration; Obtained from ERDC – Dr. Ray Chapman

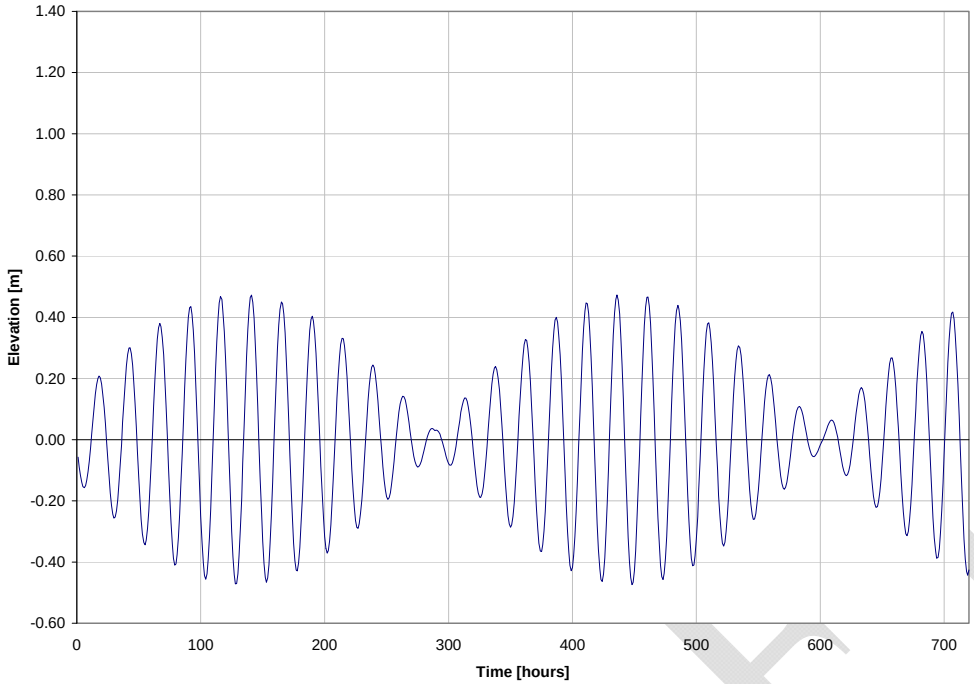

Figure 8 Normal tides forced at the Open Boundary

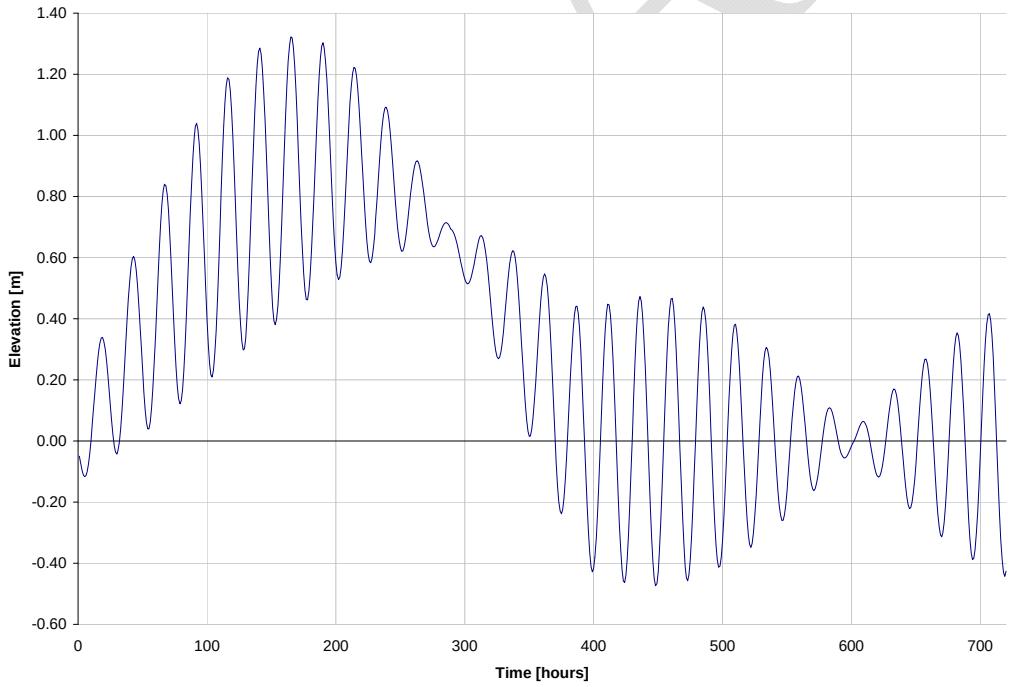

Figure 9 Extratropical surge and normal tides forced at the Open Boundary

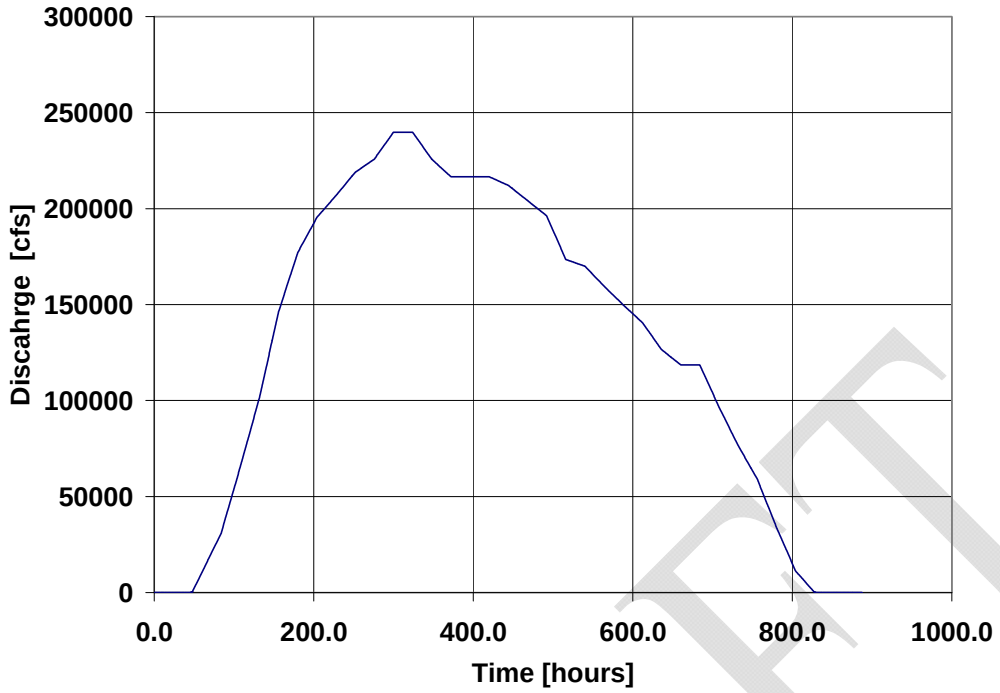

Figure 10 The 1997 Bonnet Carré Spillway Hydrograph

Available data for calibration include water levels in the interior of Lake Pontchartrain, Rigolets, Pearl River, and Pass Manchac since 1993, velocity and waves from January through May of 1998, discharge and tidal prism volumes from the tidal passes (Inner Harbour Navigation Canal – IHNC, Chef Menteur, and Rigolets) for August 1997, and salinity from monthly surveys from 1997 through 2009, and weekly salinity profiles in the vicinity of the IHNC to midlake.

Model salinities used at the open boundary represent typical historic seasonal values for the simulation period (spring season, April 1 through May 31th). These values were generated by combining: (1) discrete measurements taken in the vicinity of the boundary over the last few years by Dr. Martin O'Connell (pers. comm.), (2) extracted values from Gulf of Mexico models and Mississippi Bight models in hindcast simulations performed by the Naval Research Laboratory, Ocean Dynamics and Prediction Branch and posted on their website http://www7320.nrlssc.navy.mil/projects.php. Similar to the tidal boundary conditions, salinity boundary conditions at the open boundary were the same for all simulations.

Tributary discharges were also applied for all major rivers flowing into the Pontchartrain Basin including the Amite, Blind, and Tickfaw in Lake Maurepas, the Tangipahoa and Tchefuncte Rivers in Lake Pontchartrain, the Pearl River near the Louisiana and Mississippi State line, and the Wolf and Jordan Rivers in Bay St. Louis. Mean flows were used in the model and were based on a ten-year record from 1991 to 2001, except for the Wolf and Jordan Rivers, where monthly median flows were used based on the record length. Tributary flows are shown in Figure 11. The April flows were used in all of the comparative runs.

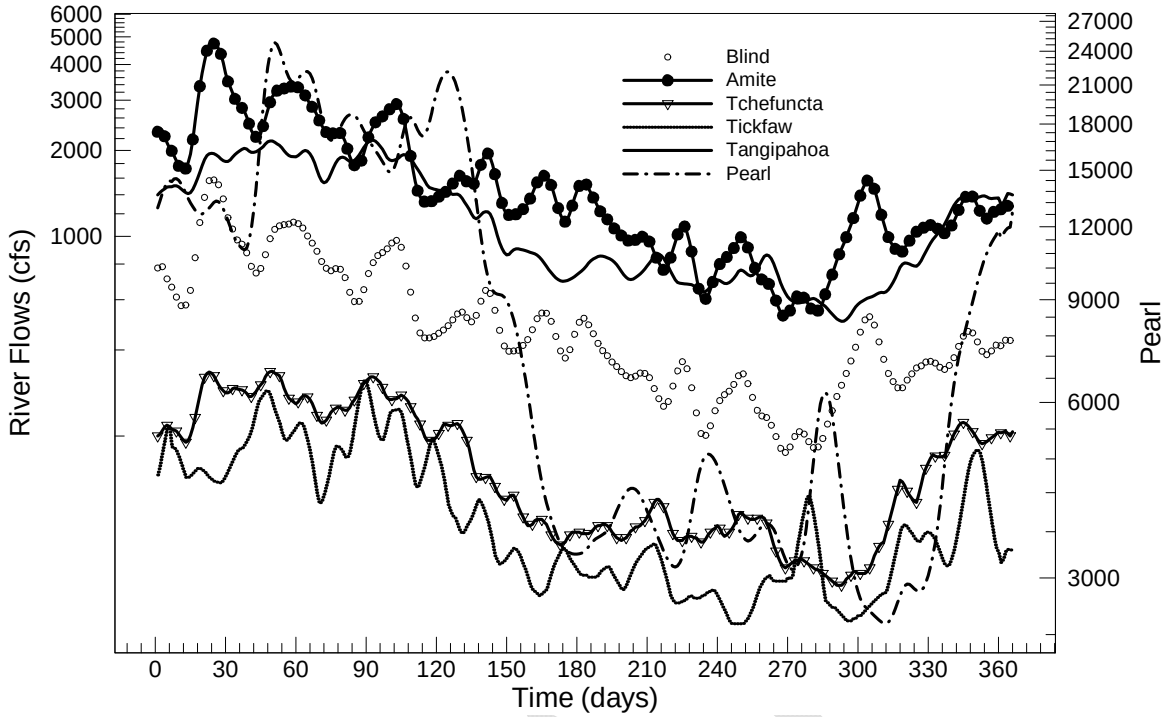

Figure 11 Tributary flows used in the model; Flows represent a 10 year average of the mean daily flow for each day. Spring flows from Jordan and Wolf Rivers are not shown here; median flows were used in the model simulations.

During 2000-2002 the USGS collected ADV, stage and salinity data at the Rigolets Pass near Lake Borgne as illustrated in Figure 12 and Appendix A. These data were useful in validating the model flows at the Rigolets.

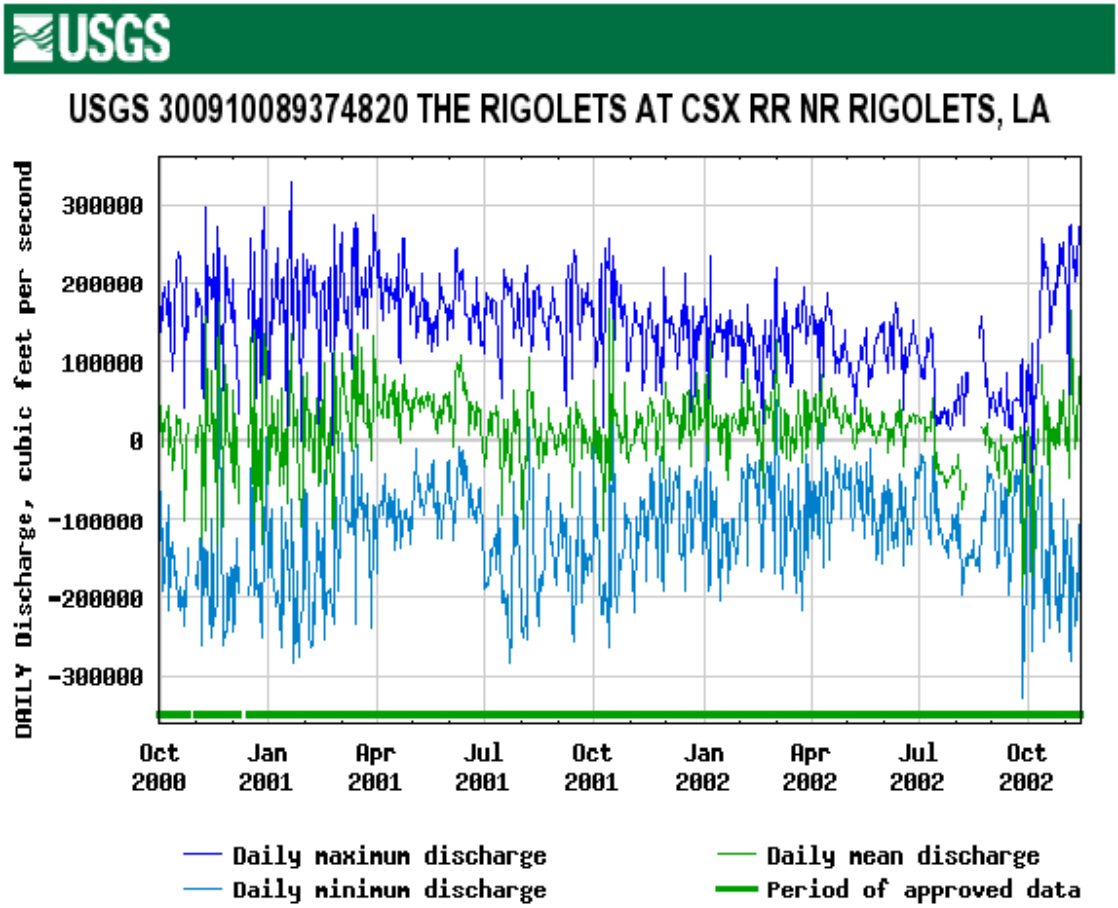

Figure 12 USGS Discharge Data for Pass Rigolets near Lake Borgne

Calibration and Validation

The model was calibrated to reproduce tidal variations throughout the basin and predicted tidal flow through the main tidal passes and the navigation complex (Intracoastal Waterway – ICWW, Inner Harbor Navigation Canal – IHNC). Discharge measurements in the tidal passes performed in August 1997 by the U.S. Geological Survey and the University of New Orleans were used to validate the model data. An Acoustic Doppler Current Profiler (ADCP) was used to collect near synoptic data across the channel. Three-dimensional velocity profiles were integrated to calculate discharge across the channel with each boat pass. The survey was completed within 2 days. The discharge data were used to compute the tidal prism through one tidal cycle. Figure 13 shows the flow distribution in thousands of cfs for each tidal pass.

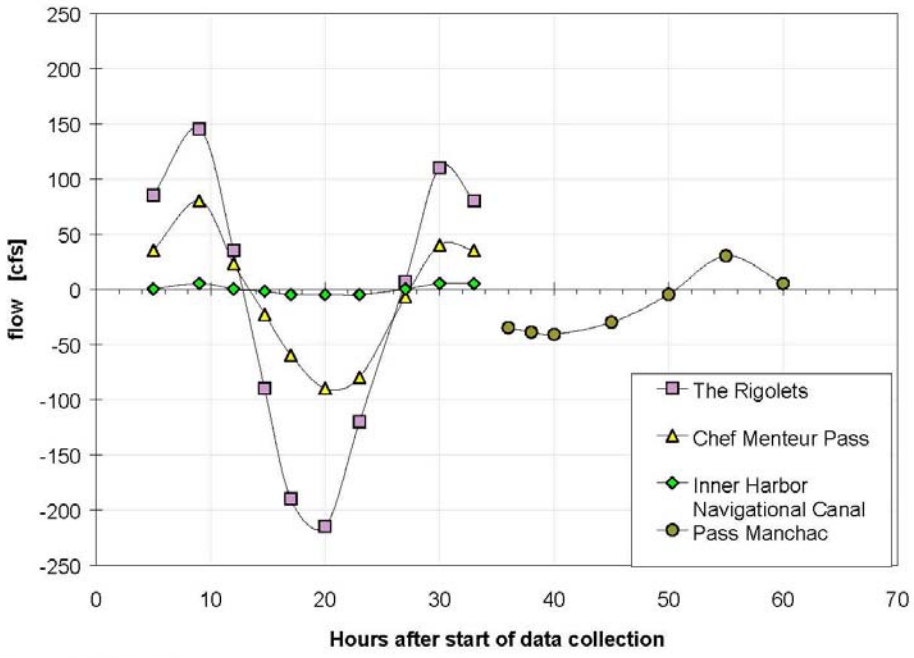

Figure 13 Tidal flow surveys through the Passes, August 1997; Flows are in 1000 of cfs (after Haralampides, 2000)

The measured flows in the tidal passes were used to calibrate the model. Local depth, elevation and velocities were extracted from the model to compute tidal flows through the passes. Parameters such as bottom roughness were varied until the desired results were obtained. A summary of the flow comparisons is shown in Table 3. Table 4 shows the comparison of the observed and simulated tidal range and phase for four locations in the interior of the basin, upstream of the tidal passes.

Table 3 Simulated and Observed flows for August 1997.

	flows in (cfs)	IHNC	Chef Menteur Pass	Pass Manchac	Rigolets	Total
Observed	Flood/Ebb	13,000	85,000	35,000	180,000	313,000
	Error (±4%)	(520)	(3,400)	(1,400)	(7,200)	(12,520)
Simulated	Flood/Ebb	15,500	82,000	36,500	175,000	309,500
	Difference	2,500	3,000	1,500	5,000	3,500

* A measurement error of less or equal to 4% of the total flow is assumed for ADCP measurements.

* Measured and simulated flow is the maximum during the tidal cycle, and is averaged for Flood and Ebb.

Table 4 Simulated and observed tidal ranges and phases for the spring tide

		Lake Pontchartrain	Rigolets Pass	Half Moon Island	Pass Manchac
Simulated	Range (m)	0.16	0.43	0.66	0.15
	Phase (hours)	23	23	24	23
Observed	Range (m)	0.17	0.31	0.65	0.16
	Phase (hours)	24	25	25	26

* Calibration for tides is based on diurnal signal.

Table 5 was derived from one year of data from a USGS ADV that was located in the Rigolets Pass. The mean of the peak daily 'flood' flows into Lake Pontchartrain was 135,000 cfs and the mean peak of the daily outflows was 170,000 cfs. The mean flood and ebb flows are approximately 150,000 cfs while the 1997 calibration data gave 180,000 cfs near the spring tide. It should be noted that the mean flow includes the flow from the West Pearl. The maximum flows in and out of the passes are the result of storm surges combined with tides. Figure 12 shows a peak outflow in 2000-2003 of over 315,000 cfs and a peak inflow of about 290,000 cfs. For modeling of high annual currents a peak flow through the Rigolets of 290,000 cfs was considered.

Table 5 Summary of Mean ADV Discharge, Salinity and Water Temperature Based on USGS Monitoring at Pass Rigolets (2000-2001)

	US System			SI System		
	Average Flood	Average Ebb	Mean	Average Flood	Average Ebb	Mean
Gage, height, ft or m	1.39	0.23	0.82	0.42	0.07	0.25
Discharge, cfs or m^3/s	169,545	-134,790	20,238	4,800	-3,817	573
Temperature, C	219	20.4	21.1			
Salinity, ppt	8.3	3.8	6.8			

Criteria for Comparison

The clear opening of the control structures for the Passes (Rigolets and Chef) have been varied from the dimensions assumed in the 1985 engineering report up to the full channel width. The criteria for judging acceptability of an option with the gates fully open are:

1. No significant change in the normal tidal prism as indicated by the change in the RMS (root mean square) with respect to the mean stage in Lake Pontchartrain. A significant change is assumed to be one that exceeds approximately 5% of the existing RMS. RMS was selected because it represents the tidal energy in the system. In addition, the effect of the existing man-made waterways on the historic tidal prism is about 5%., i.e. if all of the waterways were closed, the tidal prism in Lake Pontchartrain would be about 5% less that the existing prism (assuming no further enlargement has occurred). The existing measured flow through the IHNC is approximately 5% of the total flow through all the Passes combined; the Rigolets Pass, the Chef Menteur Pass and the IHNC.
2. There should be no significant change in the mean annual stage in Lake Pontchartrain. A one time change of more 5% of the tidal range or approximately 15 mm is assumed to be unacceptable. This is a change that could be detected by field monitoring.
3. The magnitude of the maximum velocities in the Passes in the vicinity of the structures should not be more than double the existing average velocity at the site and the fraction of the channel width where the velocities exceed the existing maximum velocities should not exceed 75% of the opening, to allow for migration of aquatic animals, i.e. 25% of the width (on average) should be available for aquatic passage.
4. The Lake Pontchartrain flushing times should not be impacted by the structures when the gates are fully open under the selected conditions 1-9.

Model Results

The FVCOM model was calibrated to reproduce the observed tidal signal in Lake Pontchartrain using boundary conditions supplied by Ray Chapman and ERDC. In addition, the model was calibrated to reproduce the observed flow distribution at the tidal passes and IHNC using ADCP observations from August of 1997.

A 1-D link-node model was used to make an initial selection for the structure openings. This model indicated that the opening should be approximately 70% of the cross-sectional area. However, this model made a number of simplifying assumptions about the velocity distribution in the vicinity of the proposed structure. The 1-D model indicated less than 5% change in the RMS of the tidal signal. The 1-D model was modified to include the acceleration terms in the links and the incremental changes in the bottom friction. Following this improvement, the model indicated that a 70% opening would result in approximately 8% decrease in the RMS of the tidal signal. The 1-D model indicated that a 1700 ft wide clear opening structure in the Rigolets Pass and a 700 ft wide structure in the Chef Menteur Pass would result in an attenuation of the tidal prism of less than 4 % compared to the existing tidal prism in the Lake with no significant difference in the mean stage.

The calibrated FVCOM was applied to the indicated 70% opening (1200 ft width in the Rigolets and 840 ft in the Chef) from the 1-D model. The FVCOM model gave a tidal RMS that was more than 10% less than the existing RMS for Lake Pontchartrain. This corresponds to over 10% attenuation of the Lake Pontchartrain neap and spring tidal ranges. The velocity distribution in the vicinity of the outflow from the structure is nearly Guassian in the FVCOM and ECOMSED simulations. This partly explains why the 3-D models gave more tidal attenuation than the 1-D model which assumes a uniform distribution of the exiting velocity across the contracted section. The FVCOM model indicated that mean stage in Lake Pontchartrain would be shifted upward by about 6 mm which represents 4.5% of the maximum tidal range. This arrangement was considered marginal in that it did not satisfy all of the criteria for insignificant change.

The calibrated FVCOM was re-run for an opening of about 86% of the cross-section area of the Rigolets at the selected site. These runs gave a tidal RMS that is approximately 5% less than the existing RMS for Lake Pontchartrain, of which about 3% is due to the shallow draft constrictions in the navigational waterways. This corresponds to about 6% attenuation of the Lake Pontchartrain spring tide of which about 3% due to proposed restrictions in the man-made waterways. The FVCOM model indicated that the mean stage in Lake Pontchartrain would be shifted by less than 1 mm which represents less than 1% of the maximum tidal range. This arrangement was considered acceptable in that it satisfied all of the above criteria. Findings from these simulations are collectively reported in Figures 14 through 23.

In particular, Figures 14 to 17 refer to a clear opening of approximately 1200 ft/700 ft Rigolets/Chef (total structure width of approximately 1400 ft/840 ft). Figure 14 indicates that there is a significant tidal attenuation for Lake Pontchartrain under normal tides (> 10%). This attenuation is greater during a Bonnet Carré Spillway opening (Figure 17). Figure 16 which compares the tides in Lake Pontchartrain with this structural open with the case of shallow draft in the navigational waterways; its noted that these time series are similar which suggests that a

significant contribution (approximately 3 – 5%) to the total tidal attenuation in Figure 14 is due to the restrictions of the waterways.

Figures 18-23 refer to the option of 1700 ft/700 ft Rigolets/Chef (total structure width of 1950 ft/840 ft). The tidal attenuation for normal tides is reduced to 6% of which 3% is due to the restricted waterways. Figure 18 shows that the Lake response to the 1997 Bonnet Carré hydrograph is very close to the base case without structures. At low Bonnet Carré flows there is almost no tidal attenuation but the attenuation is exaggerated at the peak spillway flow. Considering the infrequent operation at this high flow, this was considered to be acceptable. There is evidence of 'tidal pumping' which tends to increase the mean stage in Lake Pontchartrain, if the spring tides coincide or occur with a small phase angle relative to the corresponding peak of the spillway flow. This happens with both the existing and the structures options. The mean high stage with this structural option is about 2.5% higher than the existing; at least half of this is due to the restrictions in the waterways. Figure 19 shows that the attenuation of tides is less than 6% with a storm surge and the change in the mean stage is almost zero. The combination of a Spillway (1997) and a storm surge (~2 - 3 ft) indicated that this structural option had only a minor effect on the maximum stage in Lake Pontchartrain.

Figures 21-23 show the spring flood tide velocities at the Rigolets respectively for the existing (pre-Katrina channel), 1200 ft and 1700 ft clear openings in the Rigolets. Part of the velocity increase is due to the sill at -30 ft (NAVD88) and part is due to the constriction. The model showed that a central location of the opening avoided bank attachment of the jet of high flow. The model also indicated there is a non-uniform distribution of velocity across that opening. A high resolution 3-D in-pass model was developed for the Rigolets and Chef Passes to study the local changes in the hydraulic characteristics due to the different structural options using the ECOMSED model. The model was applied to existing conditions for peak steady state spring tidal flows as well as storm flows. The same conditions were repeated for a number of structural options. Results are reported in a later section of this report.

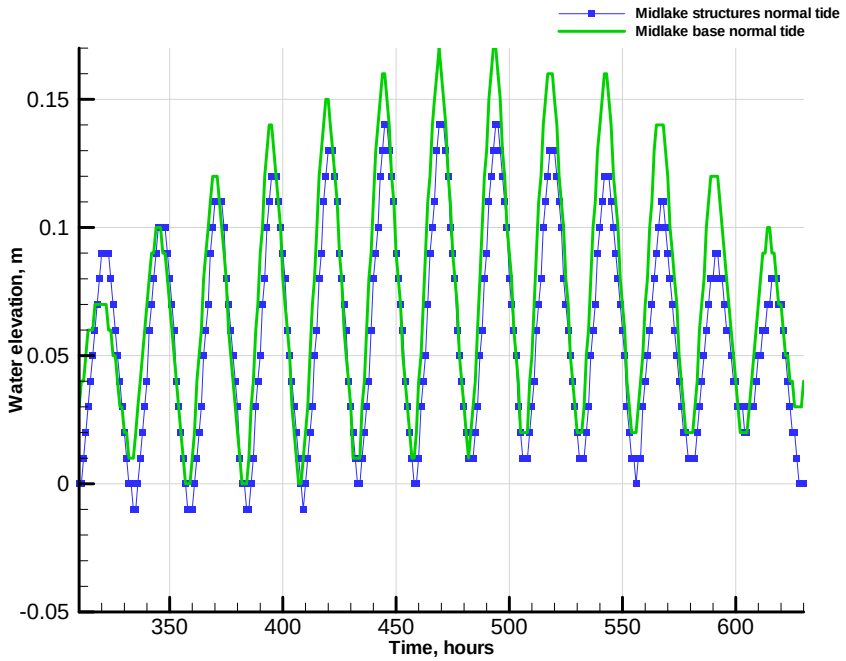

Figure 14 Comparison of the water elevation with structures and without structures for normal tide in Lake Pontchartrain (1200 ft Clear or 1400 ft total width option in Rigolets).

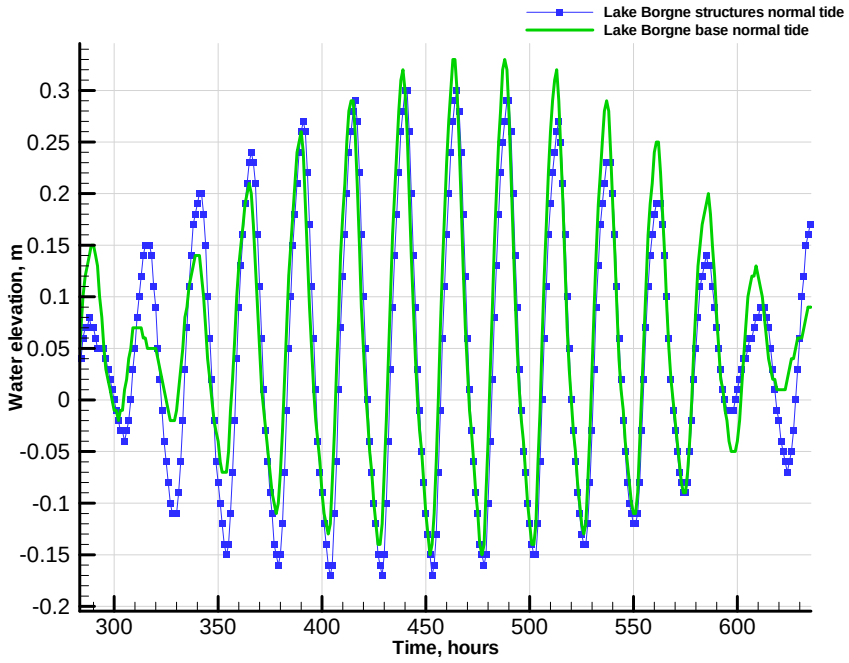

Figure 15 Comparison of the water elevation with structures and without structures for normal tide in Lake Borgne. (1200 ft Clear or 1400 ft total width option in Rigolets).

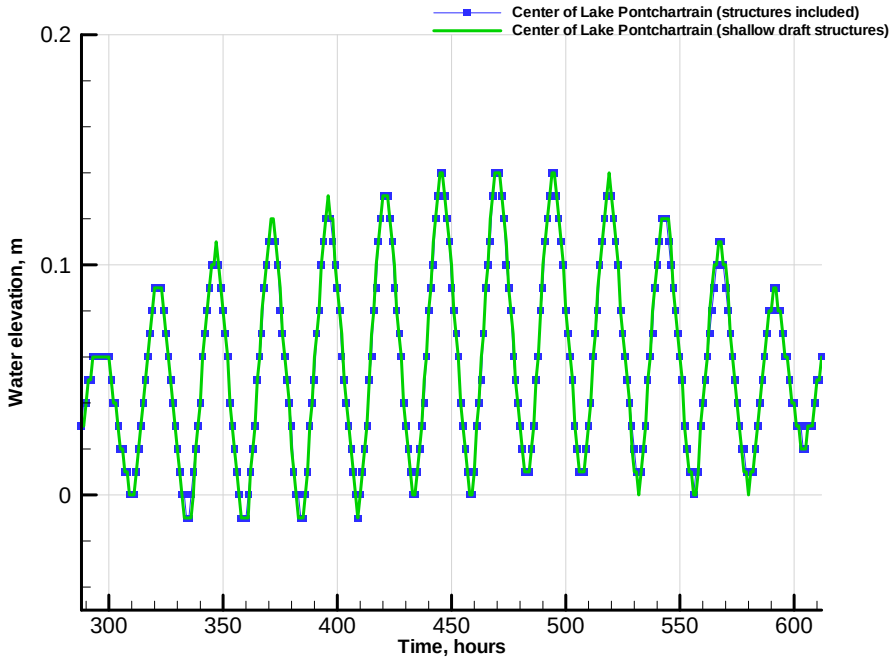

Figure 16 Comparison of the tide with structures and the tide with shallow draft on the navigation complex with normal tides in Lake Pontchartrain. (1200 ft Clear or 1400 ft total width option in Rigolets).

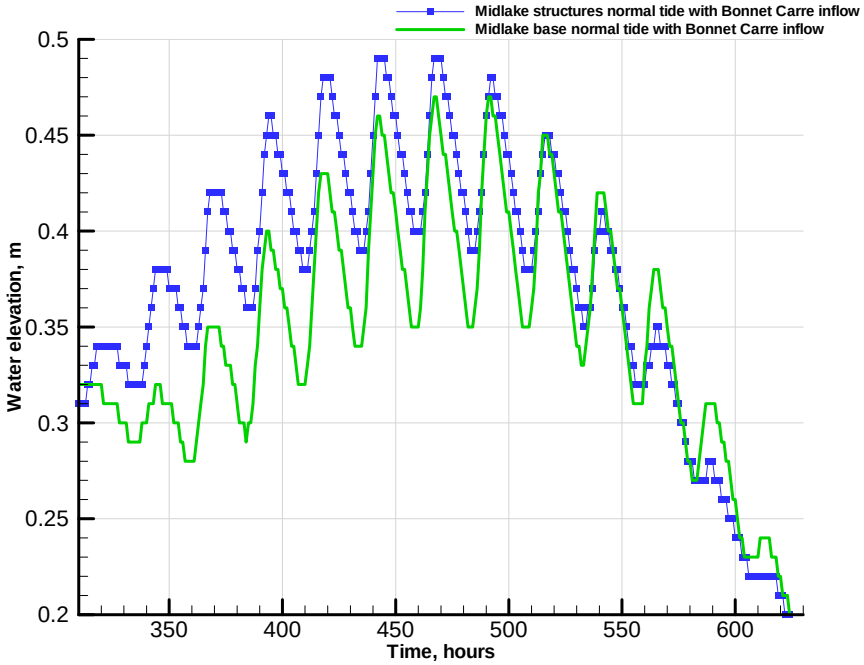

Figure 17 Comparison of the water elevation with structures and without structures for normal tide and the Bonnet Carré open in Lake Pontchartrain. (1200 ft Clear or 1400 ft total width option in Rigolets).

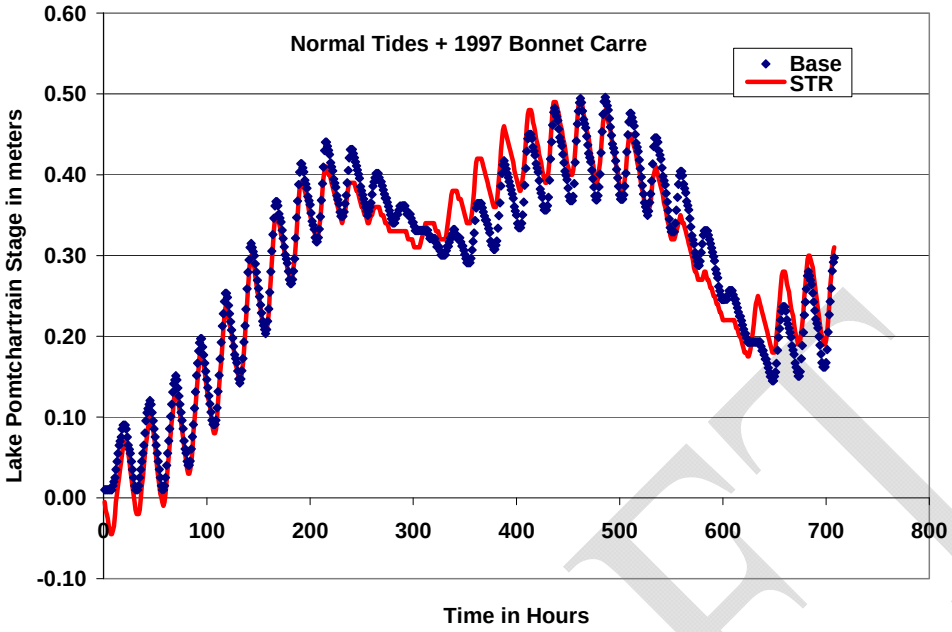

Figure 18 Comparison of the water elevation with structures and without structures for normal tide and the Bonnet Carré open in Lake Pontchartrain. (1700 ft Clear or 1950 ft total width option in Rigolets).

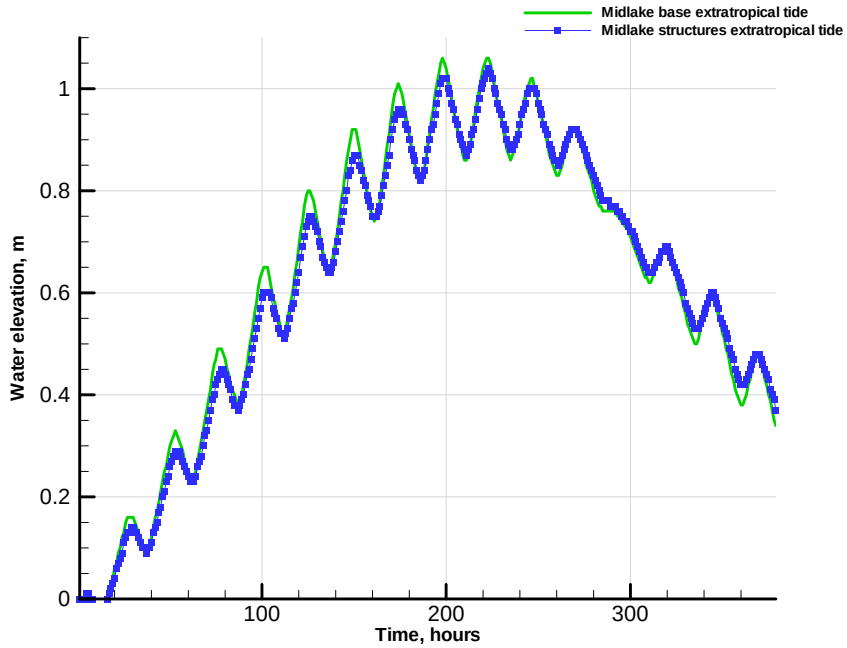

Figure 19 Comparison of the water elevation with structures and without structures for extratropical tide in Lake Pontchartrain. (1700 ft Clear or 1950 ft total width option in Rigolets).

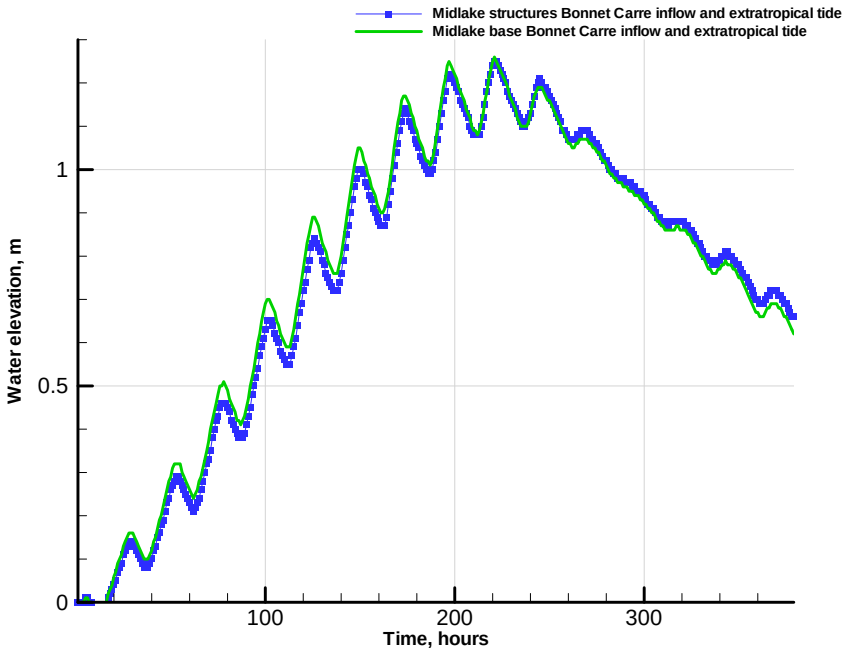

Figure 20 Comparison of the water elevation with structures and without structures for extratropical tide and the Bonnet Carré open in Lake Pontchartrain. (1700 ft Clear or 1950 ft total width option in Rigolets).

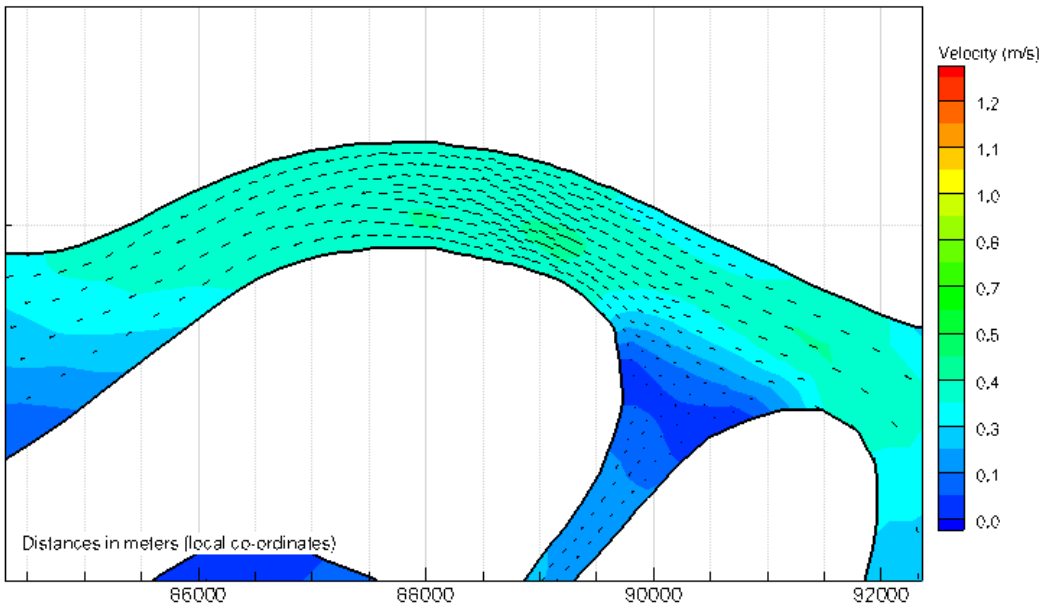

Figure 21 Existing depth-averaged velocity field at The Rigolets

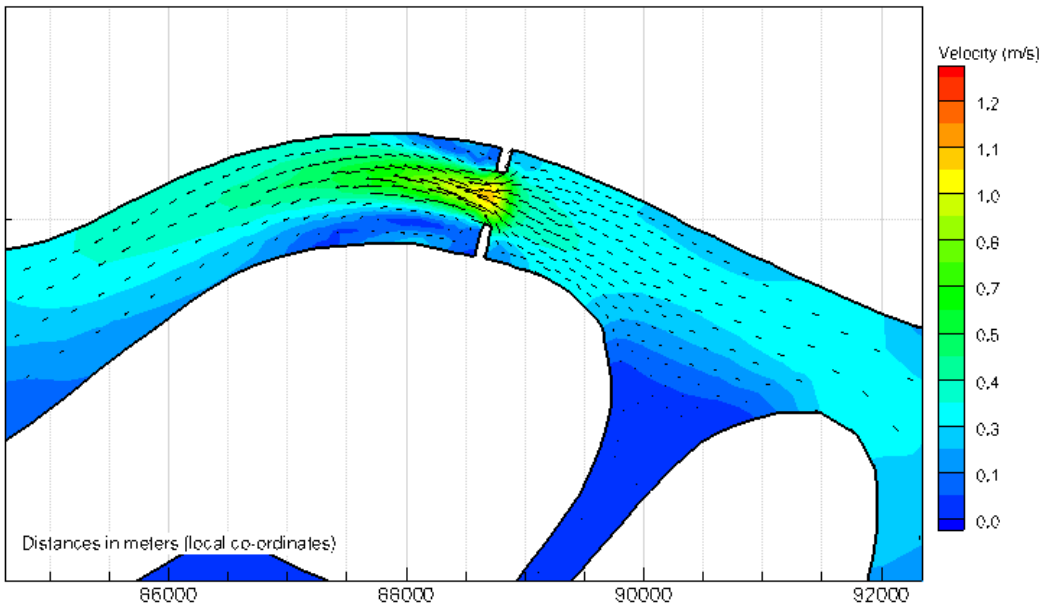

Figure 22 Depth-averaged velocity field a 1200 ft clear or 1400 ft total opening at The Rigolets

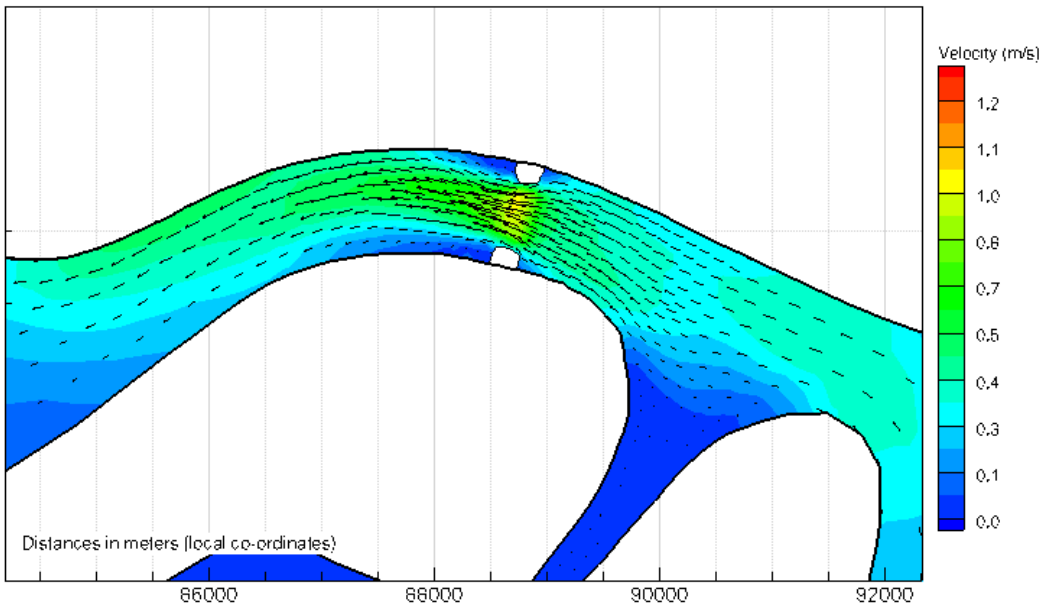

Figure 23 Depth-averaged velocity field 1700 ft clear of 1950 ft total opening at The Rigolets

High Resolution In-Pass Modeling (ECOMSED)

The Estuarine and Coastal Ocean Model with Sediments (ECOMSED) was additionally used for both the Rigolets and the Chef Menteur Passes, to better assess potential local changes in velocity, to determine head losses through the channel and proposed structures, and to obtain information on potential scour and bank protection due to higher than normal velocity field in the vicinity of the proposed structures. Models for both the Rigolets and the Chef Passes were setup as steady state with observed flow conditions.

Model Description

ECOMSED is a sigma coordinate, free surface model, designed to realistically simulate time-dependent distribution of waters levels, currents, temperature, salinity, tracers, cohesive and non-cohesive sediments and waves in oceanic and coastal systems. It is based on the Princeton Ocean Model developed by Blumberg and Mellor (1987) with modifications for its applicability in estuaries and coastal oceans by Blumberg 1996 and subsequent additions from many other contributors.

The hydrodynamic module of ECOMSED is a three-dimensional coastal ocean model, with an embedded turbulence closure sub-model to provide a realistic parameterization of the vertical mixing processes. The turbulence sub-model is a 2.5 level model that uses a prognostic equation for turbulence kinetic energy and turbulence macroscale (Mellor and Yamada, 1982). The prognostic variables are the three components of velocity, temperature, salinity, turbulence kinetic energy, and turbulence macroscale. The momentum equations are nonlinear and incorporate a variable Coriolis parameter. Prognostic equations governing the thermodynamic quantities, temperature, and salinity account for water mass variations brought about by highly time-dependent coastal upwelling/downwelling processes as well as horizontal advective processes. Free surface elevation is also calculated prognostically, with only some sacrifice in computational time so that tides and storm surge events can also be simulated. Other computed variables include density, vertical eddy viscosity, and vertical eddy diffusivity. The modeling system also accommodates realistic coastline geometry and bottom topography by the use of orthogonal curvilinear grids and sigma coordinate system.

The governing equations of the model contain propagation of fast moving external gravity waves and slow moving internal gravity waves. For computational efficiency the vertically integrated equations of the external mode are separated from the vertical structure equations of the internal mode. The governing external and internal mode equations in (x, y, σ, t) coordinate system are shown below (Blumberg and Mellor, 1987).

The Continuity Equation:

$$\frac{\partial DU}{\partial x} + \frac{\partial DV}{\partial y} + \frac{\partial \omega}{\partial \sigma} + \frac{\partial \eta}{\partial t} = 0$$

The Reynolds Momentum Transport Equations:

$$\frac{\partial UD}{\partial t} + \frac{\partial U^2 D}{\partial x} + \frac{\partial UVD}{\partial y} + \frac{\partial U\omega}{\partial \sigma} - fVD + gD\frac{\partial \eta}{\partial x} + \frac{gD^2}{\rho_o}\int_\sigma^o \left[\frac{\partial \rho'}{\partial x} - \frac{\sigma'}{D}\frac{\partial D}{\partial x}\frac{\partial \rho'}{\partial \sigma'}\right] d\sigma' = \frac{\partial}{\partial \sigma}\left[\frac{K_M}{D}\frac{\partial U}{\partial \sigma}\right] + F_x$$

$$\frac{\partial VD}{\partial t} + \frac{\partial UVD}{\partial x} + \frac{\partial V^2 D}{\partial y} + \frac{\partial V\omega}{\partial \sigma} + fUD + gD\frac{\partial \eta}{\partial y} + \frac{gD^2}{\rho_o}\int_\sigma^o \left[\frac{\partial \rho'}{\partial y} - \frac{\sigma'}{D}\frac{\partial D}{\partial y}\frac{\partial \rho'}{\partial \sigma'}\right] d\sigma' = \frac{\partial}{\partial \sigma}\left[\frac{K_M}{D}\frac{\partial V}{\partial \sigma}\right] + F_y$$

Temperature Transport Equation:

$$\frac{\partial TD}{\partial t} + \frac{\partial TUD}{\partial x} + \frac{\partial TVD}{\partial y} + \frac{\partial T\omega}{\partial \sigma} = \frac{\partial}{\partial \sigma}\left[\frac{K_H}{D}\frac{\partial T}{\partial \sigma}\right] + F_T - \frac{\partial R}{\partial z}$$

Salinity Transport Equation:

$$\frac{\partial SD}{\partial t} + \frac{\partial SUD}{\partial x} + \frac{\partial SVD}{\partial y} + \frac{\partial S\omega}{\partial \sigma} = \frac{\partial}{\partial \sigma}\left[\frac{K_H}{D}\frac{\partial S}{\partial \sigma}\right] + F_S$$

Equation of the state for the computation of density:

$\rho = \rho(\theta, S)$

$$\rho_1 = 6.76786136E-6*S^3 - 4.8249614E-4*S^2 + 0.814876577*S - 0.22584586$$

$$\rho_2 = \rho_1 * \left(1.667E-8*\theta^3 - 8.164E-7*\theta^2 + 1.803E-5*\theta\right)$$

$$\rho_3 = \rho_2 + 1 - 1.0843E-6*\theta^3 + 9.8185E-5*\theta^2 - 4.786E-3*\theta$$

$$\rho = \rho_3 * \left(6.76786136E-6*S^3 - 4.8249614E-4*S^2 + 0.814876577*S + 3.895414E-2\right)$$

Turbulent Kinetic Energy Transport Equation:

$$\frac{\partial q^2 D}{\partial t} + \frac{\partial Uq^2 D}{\partial x} + \frac{\partial Vq^2 D}{\partial y} + \frac{\partial \omega q^2}{\partial \sigma} = \frac{\partial}{\partial \sigma}\left[\frac{K_q}{D}\frac{\partial q^2}{\partial \sigma}\right] + \frac{2K_M}{D}\left[\left(\frac{\partial U}{\partial \sigma}\right)^2 + \left(\frac{\partial V}{\partial \sigma}\right)^2\right] + \frac{2g}{\rho_o}K_H\frac{\partial \tilde{\rho}}{\partial \sigma} - \frac{2Dq^3}{B_1 \ell} + F_q$$

Turbulent Macroscale Transport Equation:

$$\frac{\partial q^2 \ell D}{\partial t} + \frac{\partial Uq^2 \ell D}{\partial x} + \frac{\partial Vq^2 \ell D}{\partial y} + \frac{\partial \omega q^2 \ell}{\partial \sigma} = \frac{\partial}{\partial s}\left[\frac{K_q}{D}\frac{\partial q^2 \ell}{\partial \sigma}\right] + E_1 \ell\left(\frac{K_M}{D}\left[\left(\frac{\partial U}{\partial \sigma}\right)^2 + \left(\frac{\partial V}{\partial \sigma}\right)^2\right] + E_3\frac{g}{\rho_o}K_H\frac{\partial \tilde{\rho}}{\partial \sigma}\right)\tilde{W} - \frac{Dq^3}{B_1} + F_\ell$$

where, U is the x velocity, V the y velocity, ω the z velocity, η is the water elevation, f is the Coriolis force, D is the water depth, g is the acceleration of gravity, ρ_o is the mean density, ρ is the density, S is the salinity, T is the local temperature, θ is the potential temperature (local temperature for shallow water applications) σ is the vertical dimension (sigma levels), q^2 is the turbulent kinetic energy, and *l* is the mixing length. The density ρ is computed according to an equation of state as shown above.

The horizontal diffusion and viscosity terms are defined according to:

$$F_x \equiv \frac{\partial}{\partial x}\left(H\tau_{xx}\right)+\frac{\partial}{\partial y}\left(H\tau_{xy}\right)$$

$$F_y \equiv \frac{\partial}{\partial x}\left(H\tau_{xy}\right)+\frac{\partial}{\partial y}\left(H\tau_{yy}\right)$$

where

$$\tau_{xx} = 2A_M \frac{\partial U}{\partial x}, \quad \tau_{xy} = \tau_{yx} = A_M\left(\frac{\partial U}{\partial y} + \frac{\partial V}{\partial x}\right), \quad \tau_{yy} = 2A_M \frac{\partial V}{\partial y}$$

Also,

$$F_\phi \equiv \frac{\partial}{\partial x}\left(Hq_x\right)+\frac{\partial}{\partial y}\left(Hq_y\right)$$

where

$$q_x \equiv A_H \frac{\partial \phi}{\partial x}, \quad q_y \equiv A_H \frac{\partial \phi}{\partial y}$$

and where ϕ represents *T, S,* q^2 and $q^2 l$ (*l* is the mixing length).

The sub-grid scale processes are parameterized by the horizontal mixing coefficients. ECOMSED uses the parameterization suggested by Smagorinsky (1963) to compute the diffusivity and has the following form:

$$A_M = \alpha\Delta x\Delta y\left[\left(\frac{\partial \mathrm{u}}{\partial \mathrm{x}}\right)^2 + \frac{1}{2}\left(\frac{\partial v}{\partial x}+\frac{\partial u}{\partial y}\right)^2 + \left(\frac{\partial v}{\partial y}\right)^2\right]^{1/2}$$

Recommended value of α is 0.1 and can range from 0.01 and 0.5 for various applications.

Boundary Conditions

For both applications, boundary conditions included a free surface open boundary condition downstream and a flow boundary condition at the upstream open boundary (boundary conditions alternate depending on the simulation, e.g., downstream is the Lake Pontchartrain (west) for the flood condition, and Lake Borgne (east) side for the ebb condition. The free surface open boundary condition used in the simulations was developed by Reid and Bodine (1968), which allows long waves to radiate outside the domain with negligible reflection, and has the form of

$$\eta = \eta_0 + \frac{\lambda_t U_n}{\sqrt{g/D}}$$

where η is the sea level at the boundary and η_0 is the known water level. U_n is the model predicted velocity perpendicular to the open boundary, g is the acceleration due to gravity, and D is the depth of the grid cell. λ_t is the Lagrange multiplier and is obtained at every time step to allow modification of sea level base on the difference between computed elevation and the forced elevation at the boundary node.

For the Rigolets application, the Lake St. Catherine flow boundary condition was estimated from FVCOM for both flood and ebb conditions and the average discharge was used for all simulations. Temperature and salinity initial and boundary conditions were held constant at 25^{o}C and 8 ppt respectively for all simulations for Rigolets and Chef Menteur.

Rigolets and Chef Menteur channel model setup

The domain for this application includes the entire channel in a curvilinear orthogonal mesh, with streetwise spacing between 40 to 100 meters. The spacing in the vicinity of the structures was approximately 40 meters. This resolution allows for realistic reproduction of velocity profiles through the structure, entrainment eddies as well as good estimates of bottom applied shear stress. The mesh for the Rigolets Pass is shown in Figure 24, and it consists of 200 x 50 horizontal cells (easting and northing respectively) and 11 sigma levels with equal distribution in the vertical. All simulations were performed with full turbulent closure using the Mellor Yamada (vertical) and Smagorinsky (horizontal) turbulent closure schemes. Similarly, the Chef Menteur Pass mesh consisted of 29 x 109 x 11 sigma layers, with varying resolution from 8.5 m to 100 m in the transverse direction and 10 m to 105 m in the stream wise direction. The computational mesh for the Chef simulations is shown in Figure 25.

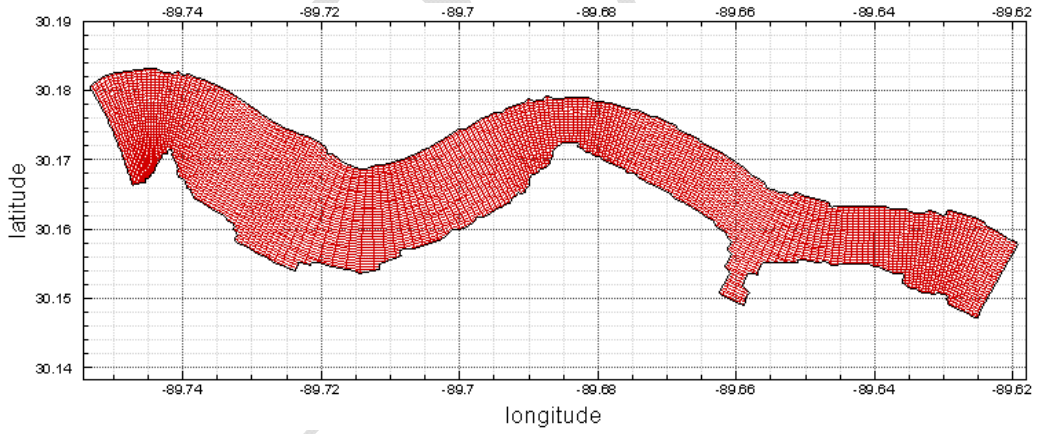

Figure 24 Computational mesh for the Rigolets simulations. The mesh consists of 200x50x11, with varying resolution of 40 to 100m in the horizontal, and 0.5 to 1 meter resolution in the vertical

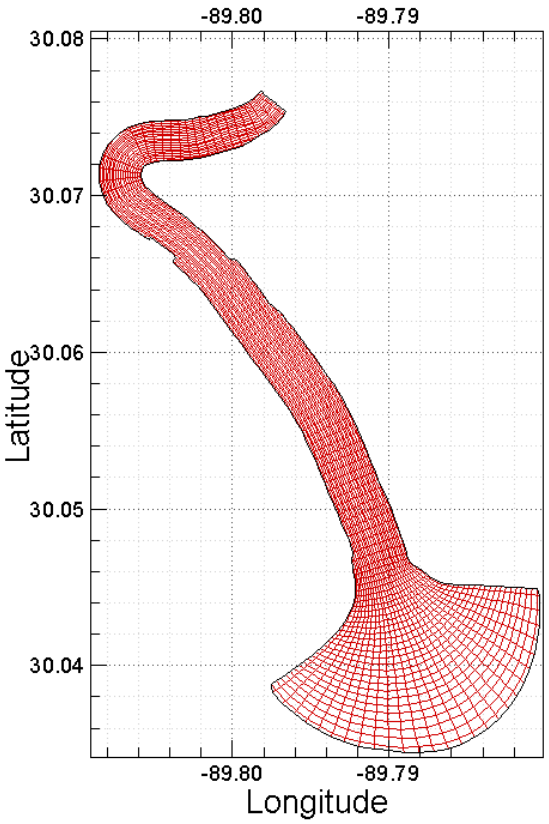

Figure 25 Computational mesh for the Chef Menteur Pass simulations. The mesh consists of 29 x 109 x 11, with varying resolution of 8.5 to 105 m in the horizontal (streamwise and transverse), and 0.35 to 1 m in the vertical.

Model results

Existing conditions (Rigolets)

For the Rigolets simulations, two scenarios were considered. The first scenario included a study of the channel under a normal maximum flow. This flow is anticipated to occur during spring tides and is approximately 185,000 cfs. Similar flows were measured under these conditions in the channel in August 1997 as shown in Figure 13. The second scenario included a much larger flow of 290,000 cfs. This flow represents the anticipated flow during an extratropical storm or an approximate mean flow resulting from a Bonnet Carré opening similar to the 1997 opening. Similar and slightly higher flows were also recorded in the entrance of the Rigolets channel near Bayou Rigolets, as seen in Figure 12. Figures 26, 27, and 28 show the resulting free surface differential stage, surface velocity magnitude and velocity head in the channel due to existing conditions with storm flow respectively. Similarly, normal spring tidal flow simulations using 185,000 cfs for both flood and ebb were carried out. Figure 29, 30 and 31 show respectively the free surface differential, surface velocity magnitude and velocity head in the channel due to existing conditions with normal flow for the flood cycle. Information collected from these simulations was then referenced as base conditions for comparisons with scenarios with selected openings.

Storm flow conditions in the Rigolets channel create a differential head loss (Figure 26) of approximately 50 cm. These conditions setup a maximum velocity pattern near the surface such as the one shown in Figure 27, with typical maximum velocities between 1.5 – 2.0 m/s. The resulting velocity head from this simulation is of the order of 10 cm. During the flood tidal cycle, the flow has the tendency to deflect towards the south bank of the channel just before the second meander (Figure 27). This flow asymmetry becomes almost normally distributed during the ebb tidal cycle, where the maximum velocity shifts northward, and it coincides with the center of the channel. The tidal flow oscillation can be exaggerated by the placement of a structure. As a result, the jet on the downstream end of the structure could become unstable, and favor either bank of the channel; a condition that can cause extensive erosion.

Under normal spring flow of 185,000 cfs, the differential head loss across the Rigolets channel is approximately half of the one we observe during storm flows. Figure 29 shows the free surface elevation across the channel, while Figures 30 and 31 show respectively the distribution of surface currents and the distribution of the velocity head. The maximum velocity under normal spring tide flows is proportional smaller to about 0.85 to 1.1 m/s. A similar trend is reflected on the velocity head in Figure 31 which is near 5 cm.

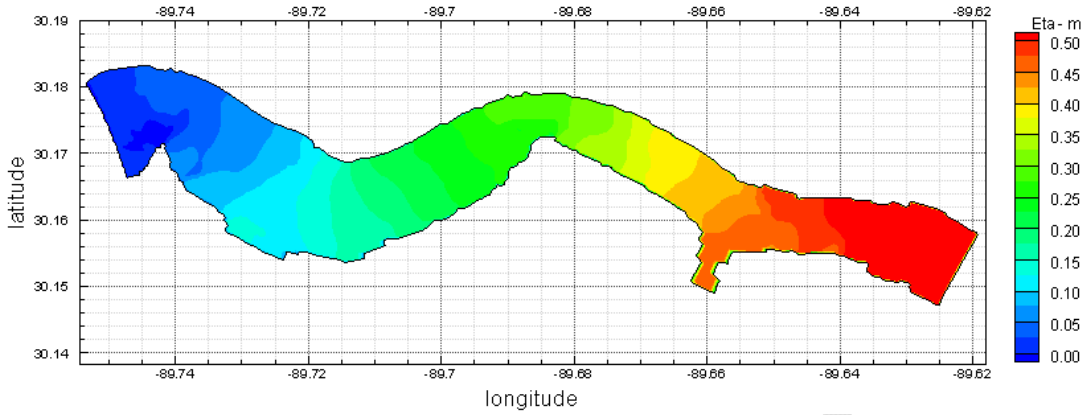

Figure 26 Differential head loss in the Rigolets channel for existing conditions and storm/flood relief flow (290,000 cfs).

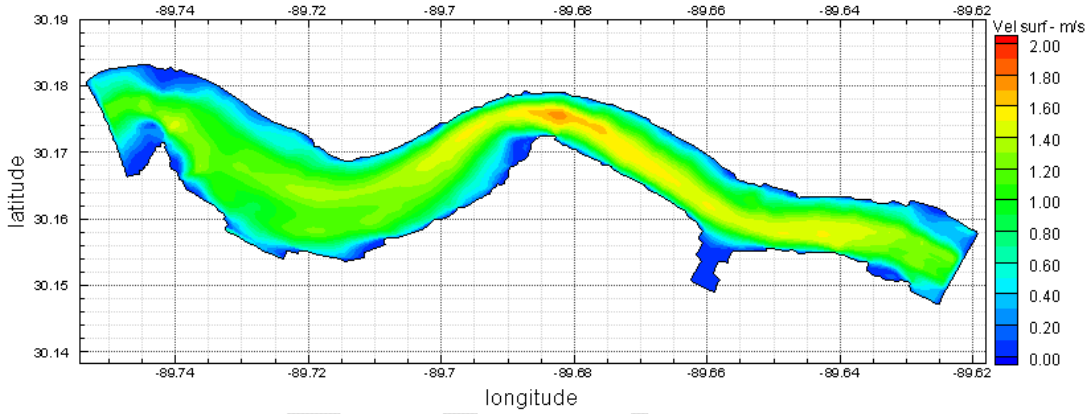

Figure 27 Distribution of surface velocities in the Rigolets channel for existing conditions and storm/flood relief flow (290,000 cfs).

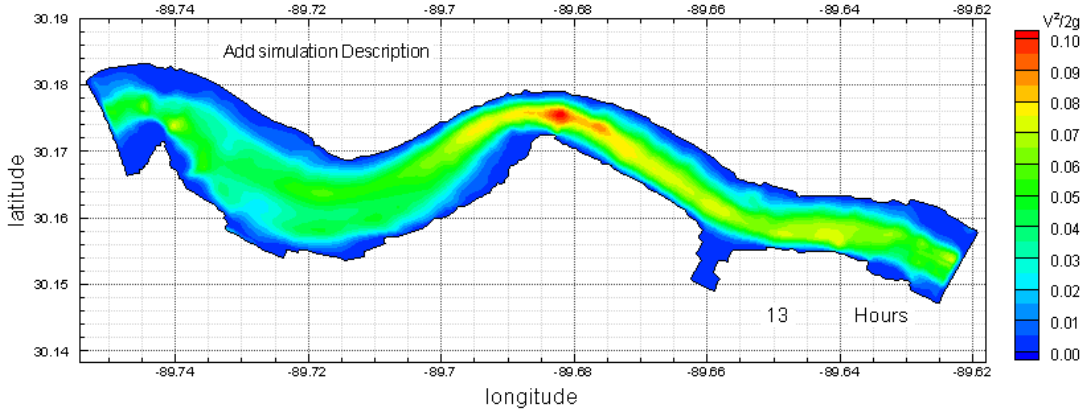

Figure 28 Velocity head ($V^2/2g$) distribution in the Rigolets Pass during flood tide and storm flow (Q=290,000 cfs).

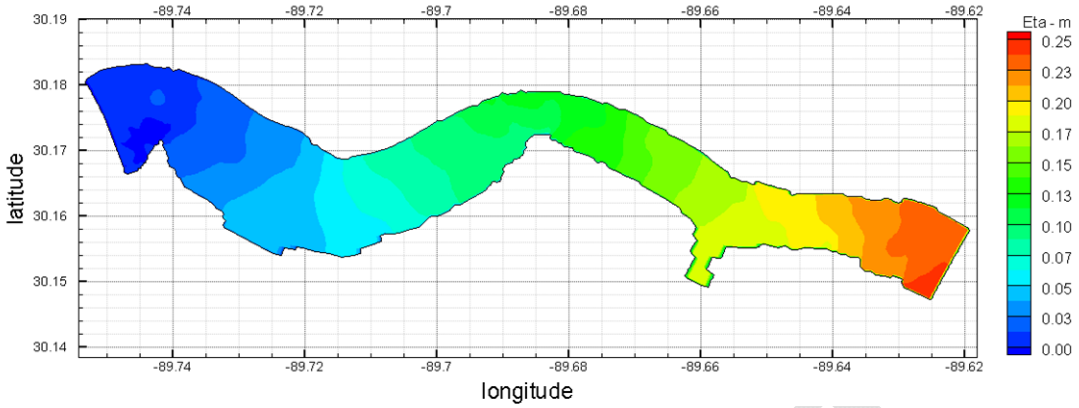

Figure 29 Differential head loss in the Rigolets channel for existing conditions and normal flow (185,000 cfs).

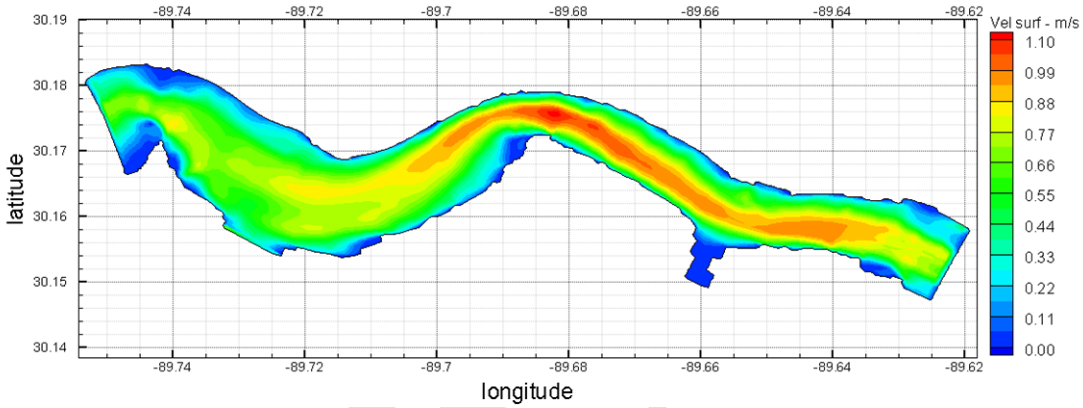

Figure 30 Distribution of surface velocities in the Rigolets channel for existing conditions and normal flow (185,000 cfs).

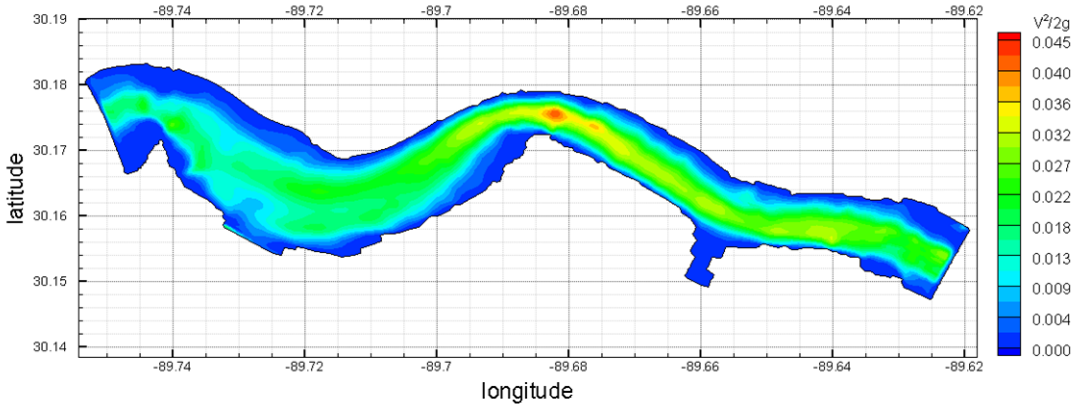

Figure 31 Velocity head ($V^2/2g$) distribution in the Rigolets Pass during flood tide and normal flow (Q=185,000 cfs).

During the ebb tidal cycle, the model predicted similar results with minor differences in the differential head of the order of 4-5 cm. The difference is mainly attributed to in-channel geometry and sequence of channel meanders, which ultimately changes fractionally the frictional losses in the channel. This change did not have a significant effect in the velocity head through the channel, and a negligible change in the maximum velocity. Figure 32 shows the distribution of free surface elevation, velocity head, differential head loss and surface velocity for existing conditions during the ebb cycle, and storm flow of 290,000 cfs through the pass.

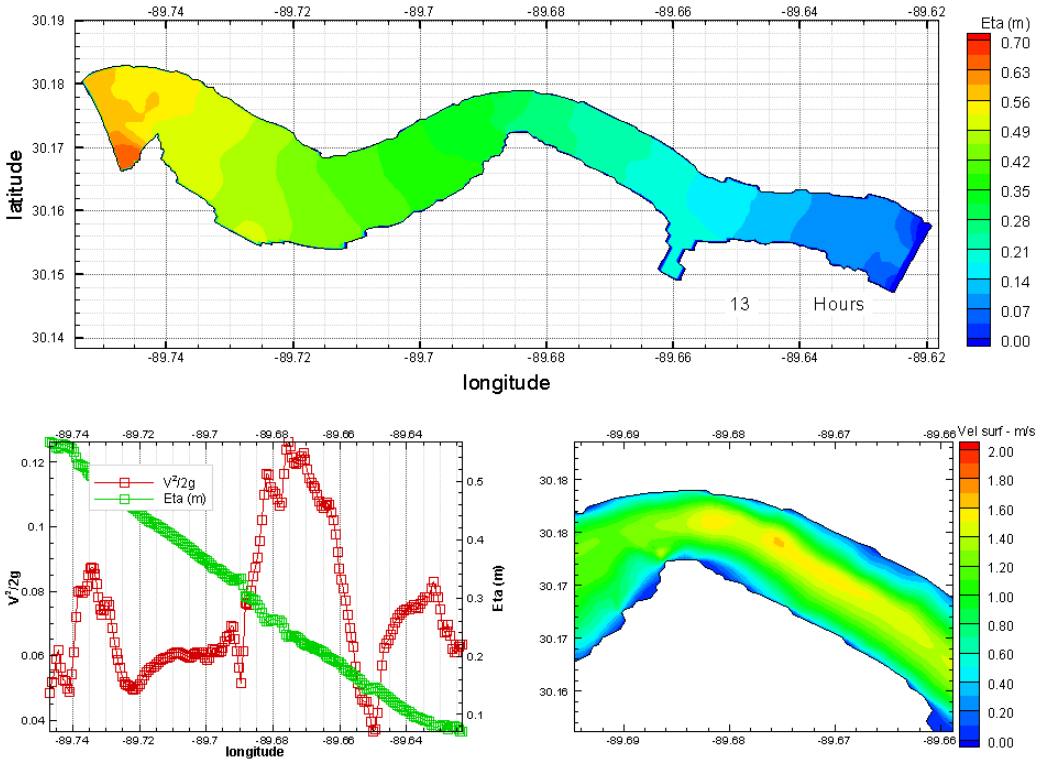

Figure 32 Distribution of free surface elevation, velocity head, differential head loss and surface velocity for existing conditions during the ebb cycle, and storm flow of 290,000 cfs through the pass.

Full Opening at Chef Menteur with New Channel

Similar to the Rigolets application, the model for Chef Menteur Pass was run with no structure in the new channel which will be excavated to accommodate for the structure as described in previous reports (USACE, 1985). The new channel is a shorter and straighter path to Lake Borgne, therefore bend and frictional losses in the channel will be less that the current conditions. However, for comparison purposes, existing conditions refer to the new channel without a structure.

Figures 33 and 34 show respectively the surface velocity distribution and the differential head loss in the channel for flood and ebb conditions. These simulations were performed as steady state with a constant flow of 85,000 cfs. For simplicity and in order to have the least contamination in the model results, the flow through the ICWW in the vicinity of the Chef Pass was neglected. This is the valid assumption because this flow would be essentially zero after completion and operation of the bypass channel.

The model predicted a head loss of the order of 15 cm across a portion of the new channel and maximum velocities of 1.3 – 1.4 m/s in the vicinity of the proposed structure.

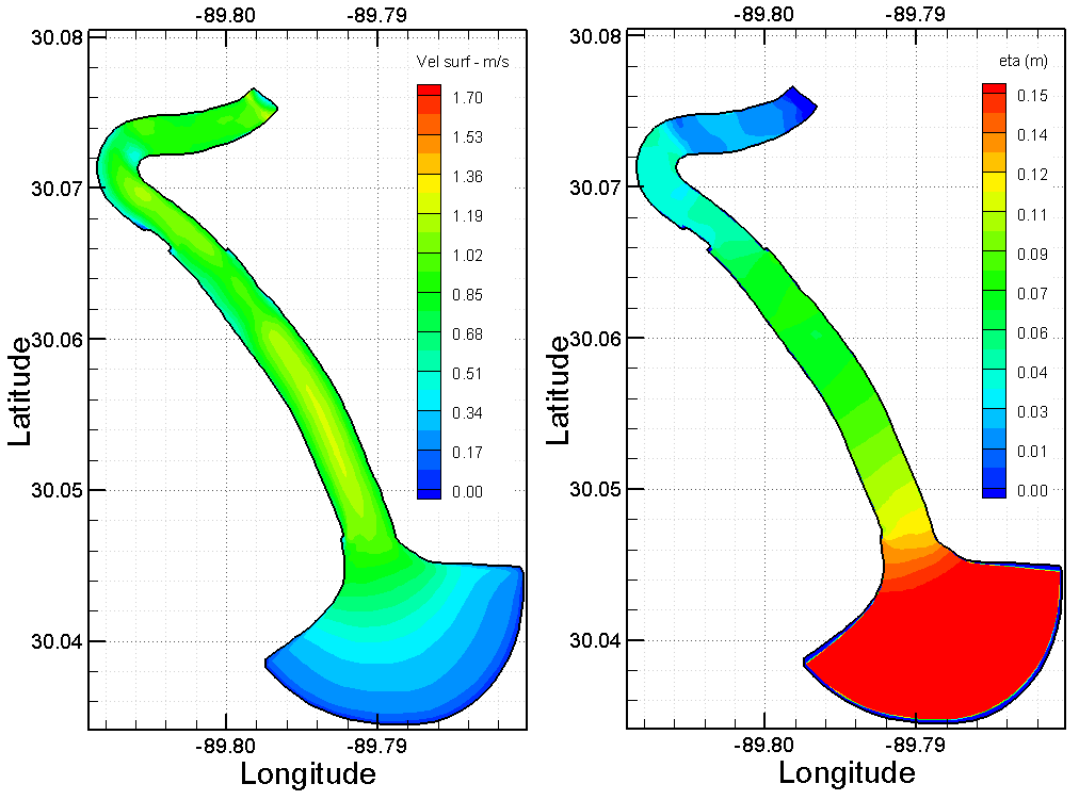

Figure 33 Distribution of surface currents and differential head loss for flood conditions in the new Chef channel; normal flow conditions of 85,000 cfs; steady state.

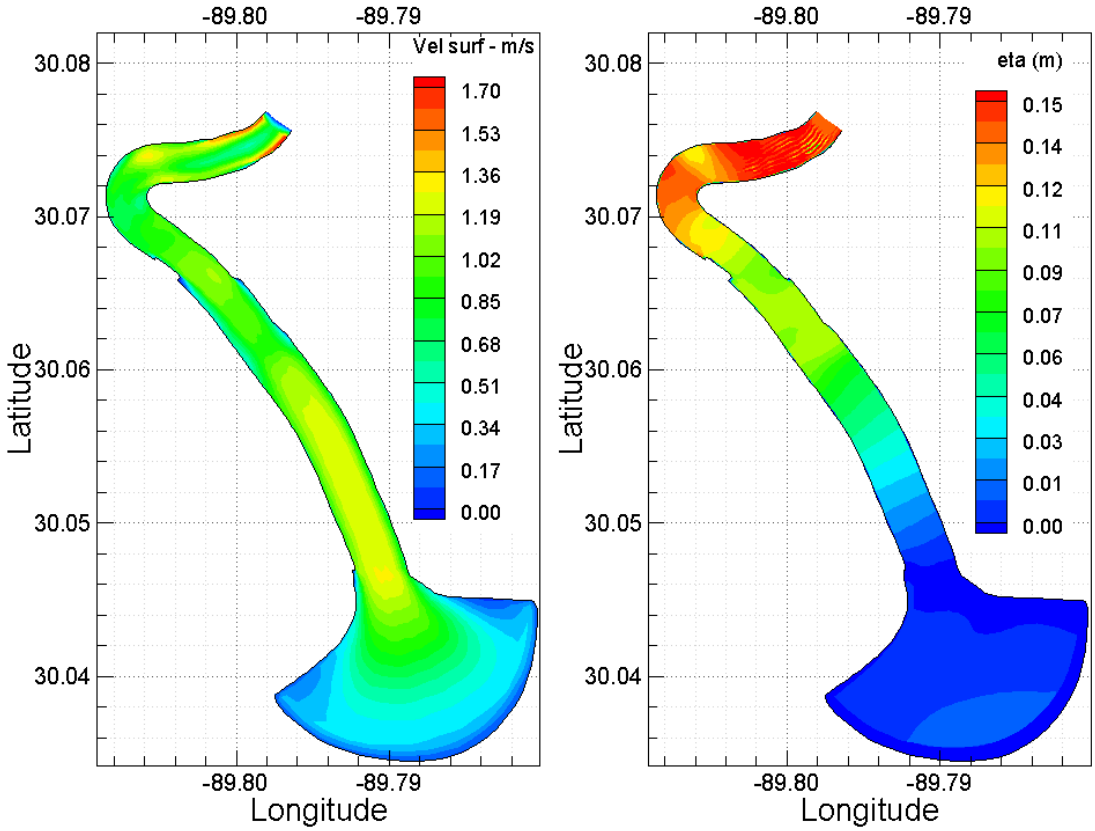

Figure 34 Distribution of surface currents and differential head loss for ebb conditions in the new Chef channel; normal flow conditions of 85,000 cfs; steady state.

Flood Control Structures

Initial structural considerations suggested by iterations using the 1-D link-node model were first considered in ECOMSED. Despite the initial predictions by the 1D link-node model, additional openings were considered, especially for the Rigolets, because it carries a proportionally higher percentage of the tidal prism.

Structures were introduced in the model by implementation of the scalar mask in ECOMSED. The mask option is used to identify the faces where fluxes are set to zero, and are thereafter treated as solid walls with a half-slip velocity boundary condition and the law of the wall assumption. Results from these simulations are shown in Figures 35 and 36, and they show the resulting free surface, velocity head, head loss and surface currents for ebb and flood tides respectively for storm flow conditions. The structure width used for these runs was 1975 ft (-30 ft NAVD 88), with no porosity, (i.e. no supporting structures between bays). Similarly to the existing case simulations, small differences are evident between flood and ebb that are attributed to primarily geometry and frictional differences.

Both simulations show maximum velocities in the vicinity of the structure of 1.6 to 1.7 m/s, and a velocity head near the structure of 11 to 12 cm. Since there are no training walls, the expanding

flow creates entrainment eddies on both sides of the structure, for both cases. The size of the entrainment eddy appears to be approximately 25% of the structure opening for this case, and of the order of 400 ft (100 m). It is noted that for this flow and an opening of 800 ft, the eddy size can be 5 - 6 times larger, approximately 2500 ft (600 m).

The constriction in the channel from this structure appears to have a free surface differential for both ebb and flood of 2 cm or 4 % of the total normal head loss. This occurs at high flows induced by extra-tropical storms or an average flow resulting from the opening of the Bonnet Carré spillway. Normal flows have a much smaller effect; less than 1 cm or less than 2 %.

Maximum velocity in the channel is typically near the surface. Increases in the surface velocity distribution are expected especially in the vicinity of the proposed structure. Local velocity increases for the 1975 ft case (Figures 35 and 36) represent a local maximum percentile increase of approximately 20% for spring tide flows; these flows occur for 2 – 3 days every lunar cycle. This change, however, occurs over a segment of the structure that is less that the 75% of the width of the opening. The maximum velocity for this structural opening is increased by 20% locally, but the increase is limited to approximately half of the structure opening; therefore, this structural arrangement satisfies the velocity criteria.

A summary of results from all simulations is shown in Table 6. Additional results with solutions for openings of 800 ft, 1500 ft and 1700 ft are shown in Appendix C. The velocity patterns for the 1700 ft clear width structure (1950 ft total width) in the Rigolets indicate the maximum velocity is less than twice the maximum without a structure and the zone for aquatic passage is about 40% of the opening. Therefore this option satisfied the velocity criteria.

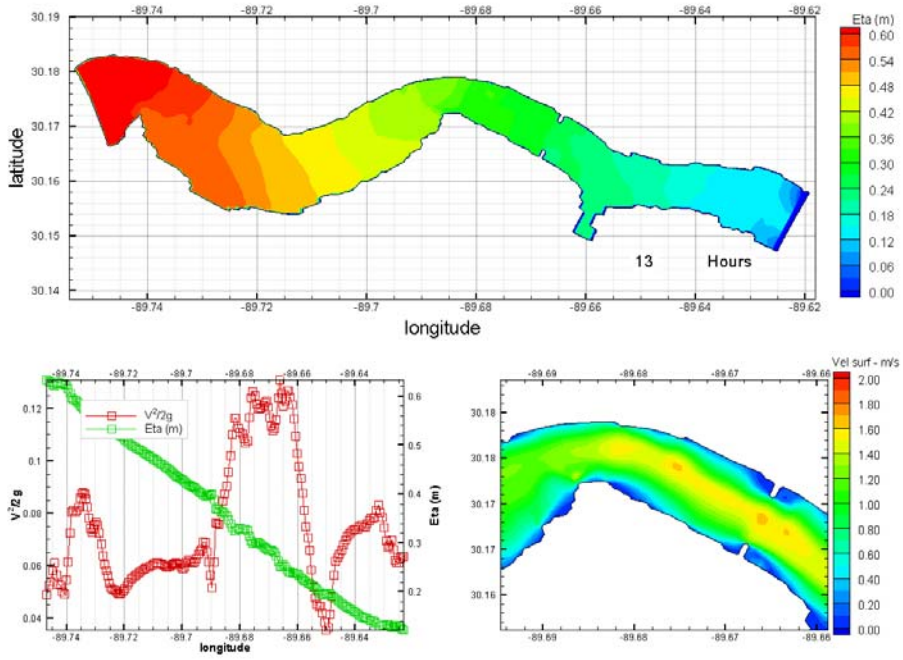

Figure 35 Distribution of free surface elevation, velocity head, differential head loss and surface velocity for a 1975 ft structure during the ebb cycle, and storm flow of 290,000 cfs through the pass.

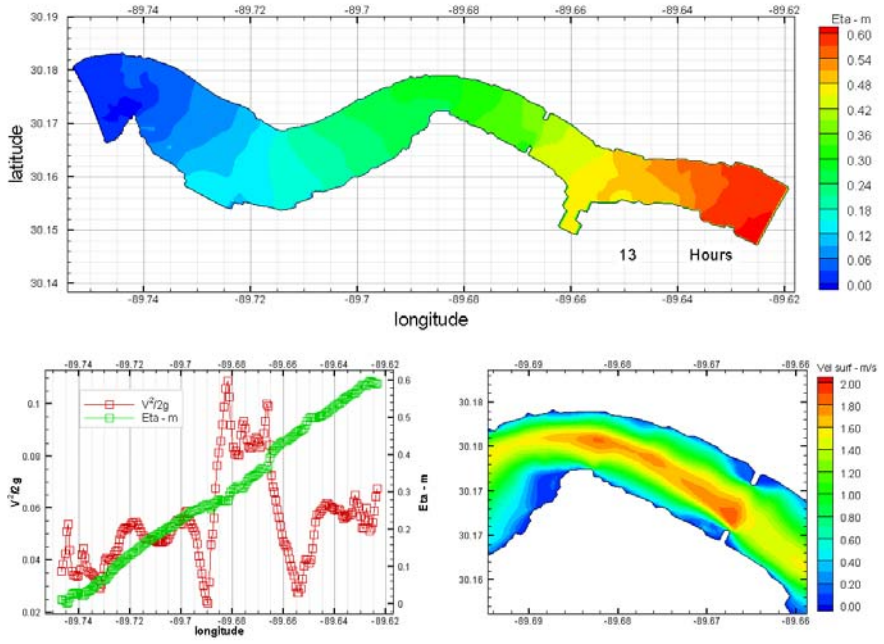

Figure 36 Distribution of free surface elevation, velocity head, differential head loss and surface velocity for a 1975 ft structure during the flood cycle; storm flow of 290,000 cfs.

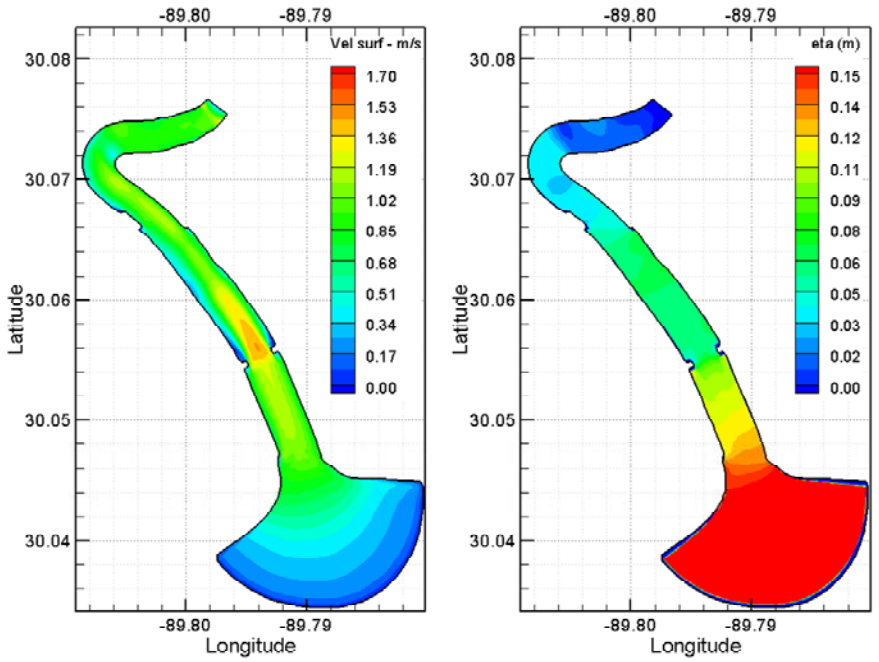

Figure 37 Distribution of surface currents and differential head loss for flood conditions in the new Chef channel with a 700 ft structure; normal flow conditions of 85,000 cfs

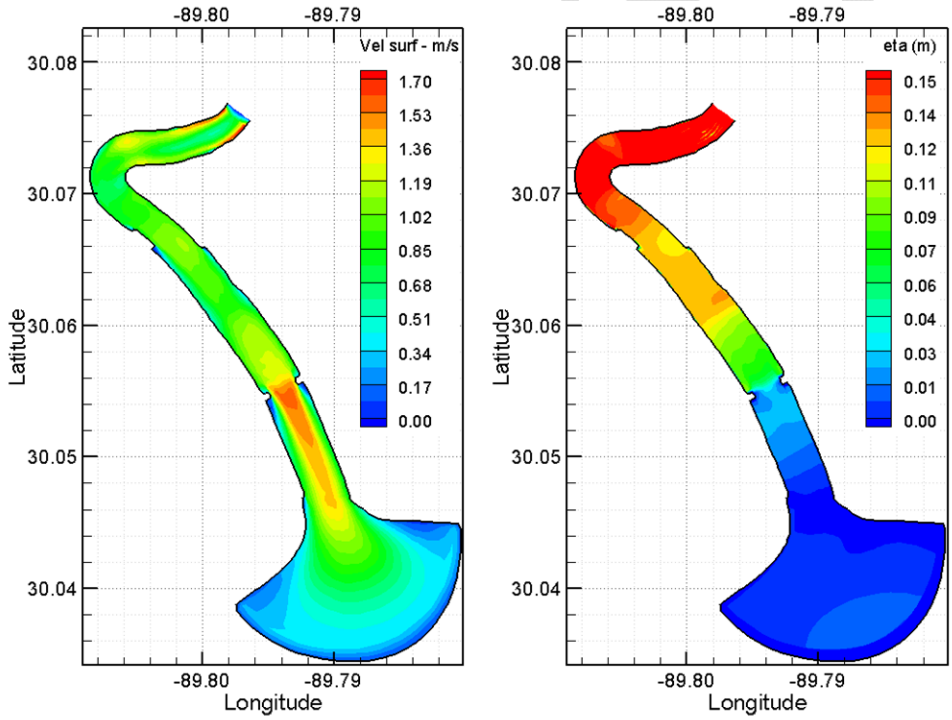

Figure 38 Distribution of surface currents and differential head loss for ebb conditions in the new Chef channel with a 700 ft structure; normal flow conditions of 85,000 cfs

Table 6 shows a summary of results from all ECOMSED simulations. The table shows the resulting increase in head loss for each of the structures tested, the resulting maximum velocity head and the maximum velocity.

Table 6 Summary of results from in-pass simulations with ECOMSED.

Location	Conditions or opening size	Flow direction	Flow (cfs)	Differential Head (cm)	$V^2/2g$ (cm)	V_{max} (m/s)
Rigolets	Existing	Flood (spring)	185,000	24.8	4.2	1.00
Rigolets	Existing	Ebb (spring)	185,000	25.0	5.0	1.00
Rigolets	Existing	Flood (maximum)	290,000	58.0	10.0	1.50
Rigolets	Existing	Ebb (maximum)	290,000	48.0	12.5	1.55
Rigolets	1975 ft	Flood (spring)	185,000	25.0	4.4	1.20
Rigolets	1975 ft	Ebb (spring)	185,000	25.0	5.2	1.36
Rigolets	1975 ft	Flood (maximum)	290,000	60.0	10.7	1.85
Rigolets	1975 ft	Ebb (maximum)	290,000	50.0	13.0	1.60
Rigolets	800 ft	Flood (maximum)	290,000	137.0	75.0	4.30
Rigolets	1700 ft	Flood (maximum)	290,000	64.0	14.0	2.05
Rigolets	1500 ft	Flood (maximum)	290,000	68.0	20.0	2.25
Chef Menteur	1000 ft	Flood (spring)	85,000	16.7	7.5	1.20
Chef Menteur	1000 ft	Ebb (spring)	85,000	14.5	7.5	1.23
Chef Menteur	700 ft	Flood (spring)	85,000	18.5	10.5	1.44
Chef Menteur	700 ft	Ebb (spring)	85,000	15	12	1.55

In order to test whether the maximum velocity criteria are met within the channel for the passage of aquatic animals, hydraulic features were extracted from each available solution and are shown in Table 7. This table shows, for each case that was simulated, the ratio of the maximum velocity to the average normal velocity occurred under spring tides. Additional information includes the relative percentile increase of the maximum velocity to the normal velocity, the impact width of that velocity reported as normalized percentage of the structure opening, and the average eddy dimensions normalized as a percentage of the structure width. The model results, shown in summary Table 7, clearly show that eddy structures can vary in diameter from 400 ft to more than 3000 ft. The model also suggests that to meet the criterion of the maximum velocity (not to exceed by a factor of 2 the average velocity at the site), the recommended total width of the structure should be in the neighborhood of 1950 ft or 1700 ft clear opening. Moreover, this is the smallest width of structure that meets the width requirements for the maximum velocity exceedences.

Table 7 Summary of hydraulics features in the Rigolets Pass as a results of Structures

Location	Conditions or opening size	Flow direction	Flow (cfs)	Vmax/Vavg ratio	Vmax (% increase)	Impact Width Percent of Opening	Eddy Size as Percent of opening
Rigolets	Existing	Flood	185,000	1.2	16.7%		
Rigolets	Existing	Ebb	185,000	1.3	23.1%		
Rigolets	Existing	Flood	290,000	1.2	16.63%		
Rigolets	Existing	Ebb	290,000	1.3	23.%		
Rigolets	1975 ft	Flood	185,000	1.5	33.3%	60	25
Rigolets	1975 ft	Ebb	185,000	1.55	35.5%	60	25
Rigolets	1975 ft	Flood	290,000	1.85	45.9%	60	20
Rigolets	1975 ft	Ebb	290,000	1.6	37.5%	60	20
Rigolets	800 ft	Flood	290,000	4.3	76.7%	90	500
Rigolets	1700 ft	Flood	290,000	2.0	51.2%	62	80
Rigolets	1500 ft	Flood	290,000	2.2	55.6%	75	250
Chef Menteur	1000 ft	Flood	85,000	1.3	23%		
Chef Menteur	1000 ft	Ebb	85,000	1.3	23%		
Chef Menteur	700 ft	Flood	85,000	1.20	30.6%	60	80
Chef Menteur	700 ft	Ebb	85,000	1.3	35.5%	60	80

[1] Impact width and Eddy size are normalized to the proposed/reference structure for each case

The proposed structure at the Chef Pass involves the construction of a new shorter and straighter channel which has lower bend and lower friction losses. Table 8 shows the estimated differences in the head losses at spring tide of approximately 85,000 cfs. The losses are compared to the existing channel. The computations show that the new channel would result in a reduction in the head loss of 0.23 ft. The new channel with a structure having a 700 ft opening would have almost the same resistance to flow as the existing channel. A 750 ft opening would result in a 0.07 ft lower head loss than the existing channel. Since the total head loss in the Chef Pass at 85,000 cfs is approximately 1 ft, the 750-ft opening would result in about 7% less resistance than the existing channel. This analysis is for the head loss for the part of the Chef Pass on the Reach between the ICWW and Lake Borgne.

Table 8 Effect of New Channel and Structures on Head Losses during a Spring Tide

Case	Opening Ws ft	Loss [ft]	Difference in Loss Compared to Existing Channel [ft]
Existing	1000	0.39	0.00
New	1000	0.16	-0.23
New + Chef structure	600	0.59	0.20
New + Chef structure	700	0.39	0.00
New + Chef structure	750	0.33	-0.07
New + Chef structure	840	0.23	-0.16

Table 9 was developed for the case of modifications to the Chef Pass with the existing Rigolets Pass. The Table indicates that the tidal prism could increase by about 5% if the new straighter and shorter channel were constructed without encroachment by a structure. A 750-ft opening would result in less than 2% increase in the tidal prism.

Table 9 Effect of New Straighter and Shorter Channel on Tidal Prism with the Existing Rigolets Channel and Various Options in the Chef Pass

Case	Opening Ws ft	Q1 1000cfs	Q2 1000cfs	QT 1000cfs	Factor on Tidal Prism
Existing	1000	195	85.0	280.0	1.00
New	1000	195	99.0	294.0	1.05
New + Chef structure	600	195	77.2	304.3	0.97
New + Chef structure	700	195	85.3	262.5	1.00
New + Chef structure	750	195	88.6	284.3	1.02
New + Chef structure	840	195	94.4	297.7	1.04

Discussion and Conclusions

The selection of structures that meet the criteria for insignificant impacts involves:

- examining the results of the FVCOM model for changes in the tidal prism under normal diurnal tides over a lunar period.,
- examining the local velocity patterns as simulated by ECOMSED,
- reviewing the impacts of the structures on the Lake Pontchartrain during extratropical storm surges and the operation of the Bonnet Carré Spillway.

The FVCOM simulations showed that introducing shallow draft restrictions in the Intracoastal Waterway, IHNC and MRGO would reduce the existing tidal prism by approximately 3%. Total closure would reduce the tidal prism by as much as 5%, i.e. the historic tides in Lake Pontchartrain were probably 5% lower before the construction of the navigational waterways. The model indicated that the shallow draft option for the navigational waterways (IHNC, ICWW and MRGO) would reduce the existing tidal prism in Lake Pontchartrain by 3%.

Combining the results from the ECOMSED and FVCOM, the tidal prism attenuation between Lake Borgne and Lake Pontchartrain was computed as shown in Table 10. From this Table it appears that a structure with a clear opening of 1700 ft in the Rigolets and 700 ft in the Chef Menteur Pass satisfies the criterion of less than 5% decrease in the tidal prism of Lake Pontchartrain. Of this attenuation approximately 3% is due to the shallow draft restrictions in the waterways. The dimensions for the structures shown in Table 10 are selected to maintain the present flow split between the Rigolets and the Chef. The increase in the stage of Lake Pontchartrain under normal tidal forcing is less than 1% for the option of 1700 ft (clear) at Rigolets and 700 ft (clear) at Chef Pass based on clear openings with shallow draft restrictions in the waterways. For the Bonnet Carré Spillway (1997) event the increase in stage is less than 3% of the normal increase in depth. Similar stage changes are indicated for the combined spillway and extratropical storm surge for the above structural option.

Table 10 Summary of Tidal Attenuation Between Lake Borgne and Lake Pontchartrain

Rigolets feet Clear	Chef feet Clear	WW	Attenuation
2300	1000	Open	0
2300	1000	Shallow	3
2300	1000	Closed*	5
800	420	Open	31%
800	420	Shallow	33%
1500	600	Open	11%
1500	600	Shallow	14%
1700	700	Open	2%
1700	700	Shallow	4%
1700	700	Closed*	6%
1975	840	Open	0.5%
1975	840	Shallow	3.5%

* Based on measured flow in IHNC.

The ECOMSED model showed that a 1700 ft structure in the Rigolets resulted in less than a 25% increase in the maximum velocities (maximum velocity = 2 x the average velocity) and at least 25% of the cross-section with velocities equal or less than the maximum currents that would exist without the structure. The distance downstream of the entrainment eddies between the exiting flow from the structure and the channel banks are reduced to less than one opening.

The scour patterns at existing structures in the Passes can be used as an indicator of the localized shear stress patterns that can result from the presence of a structure in the Passes. Exaggerated scour depths resulted from the storm surge and subsequent outfall due to Hurricane Katrina were recorded. The storm surge including wind setup on Lake Pontchartrain was estimated to be about 12 ft. In less than 2 days the stage in the Lake dropped to approximately 4 ft or a decrease of about 8 ft on the south shore. Assuming that setup was of the order of 3 ft, the volume of outflow was approximately the Lake surface area of 1640 km^2 times a depth of about 5 ft (1.5m). The outflows from Lake Pontchartrain were estimated using this volume and recession time of 24 hours. As indicated in Table 11, the outflow following Katrina was more than double the normal spring tide flow. The estimated channel velocities are similarly increased. As indicated by the post-Katrina multibeam images, this resulted in severe scour in both Passes. For example, there was over 116 ft of scour in the Chef Pass in some locations such as at the railway bridge in the Chef Pass and at channel bends. Figure 39 shows the erosional remnants at the railway bridge across the Chef Pass due to 'storm surge' into Lake Pontchartrain and the outflow of the stored water after Katrina. The scour pattern is asymmetrical on the outflow side. Similar scour patterns are expected at pier supported structures in the Passes. The selected sites in the Chef and Rigolets channels produce nearly symmetric high velocity zones (Figures 36, 37 and 38) which should produce a more symmetrical scour pattern than that shown in Figure 39.

Table 11 Estimated Outflow through the Passes Following Hurricane Katrina

	Measured Qmax (tidal) cfs	**Flow Distribution**	**Estimated Katrina Q cfs**	**V ft/sec**	**Nf**
Rigolets	190,000	0.66	450,000	~7	~0.2
Chef	85,000	0.29	200,000		
IHNC	14,000	0.05	30,000		
Total	289,000		~680,000		

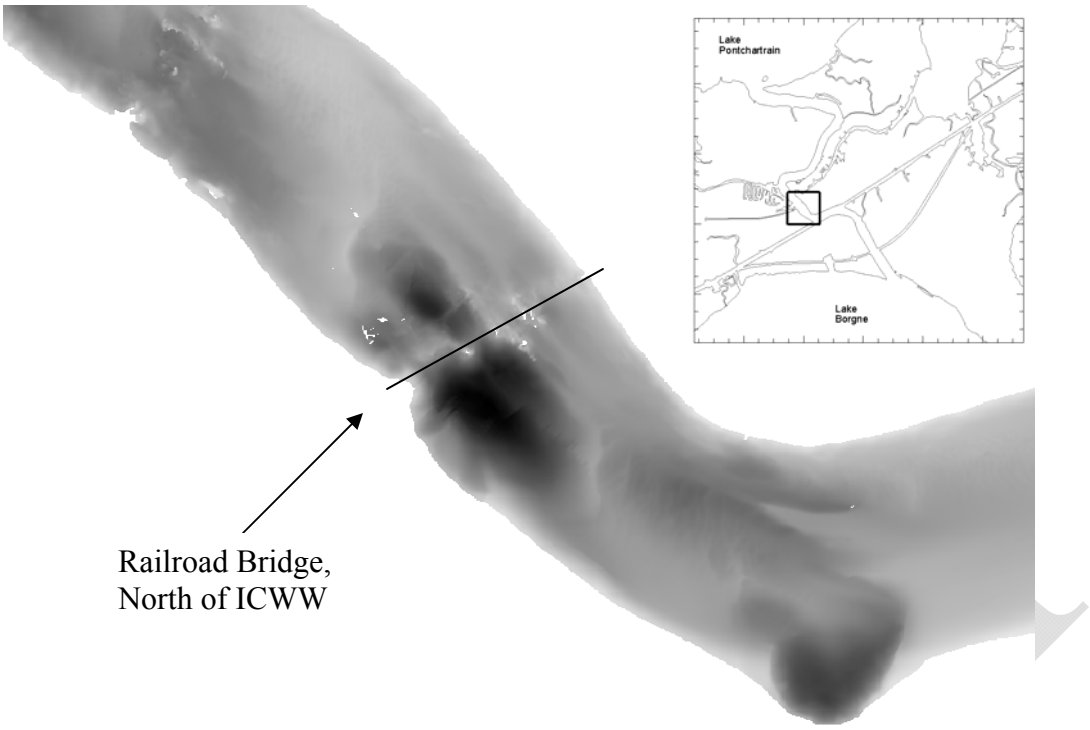

Figure 39 Scour pattern in the Chef Pass downstream of a Railroad Bridge with Piers due to outflow from Hurricane Katrina (dark colors represent soundings of over 100 ft; mid-grey tones represent soundings of 60 – 75ft, and light tones less than 50 ft)

Table 12 shows the suggested structural opening that are required to avoid significant changes in the tidal prism of Lake Pontchartrain.

Table 12 Suggested Structure Sizes to Avoid Changes in the Tidal Prism

Location	**Clear Width [ft] (Total structure width)**	**Sill [ft] NADV88**	**Comments**
Rigolets	1700 (1950)	-30	West of ICWW
Chef Menteur	700 (790)	-30	New 1000 ft wide channel from ICWW to Lake Borgne
MRGO	150	-15	South of Violet
ICWW	150	-12	Several Locations as Shown in Figure 2
IHNC	150	-12	Near Lake Pontchartrain
Lake Catherine			By-passing Blocked by levee

A generic structure has been assumed in the estimation of the closure dimensions. Figure 40 shows the structure that was assumed for this study. The dimensions derived from the model are the clear widths for the Rigolets and Chef Passes as shown in Table 13.

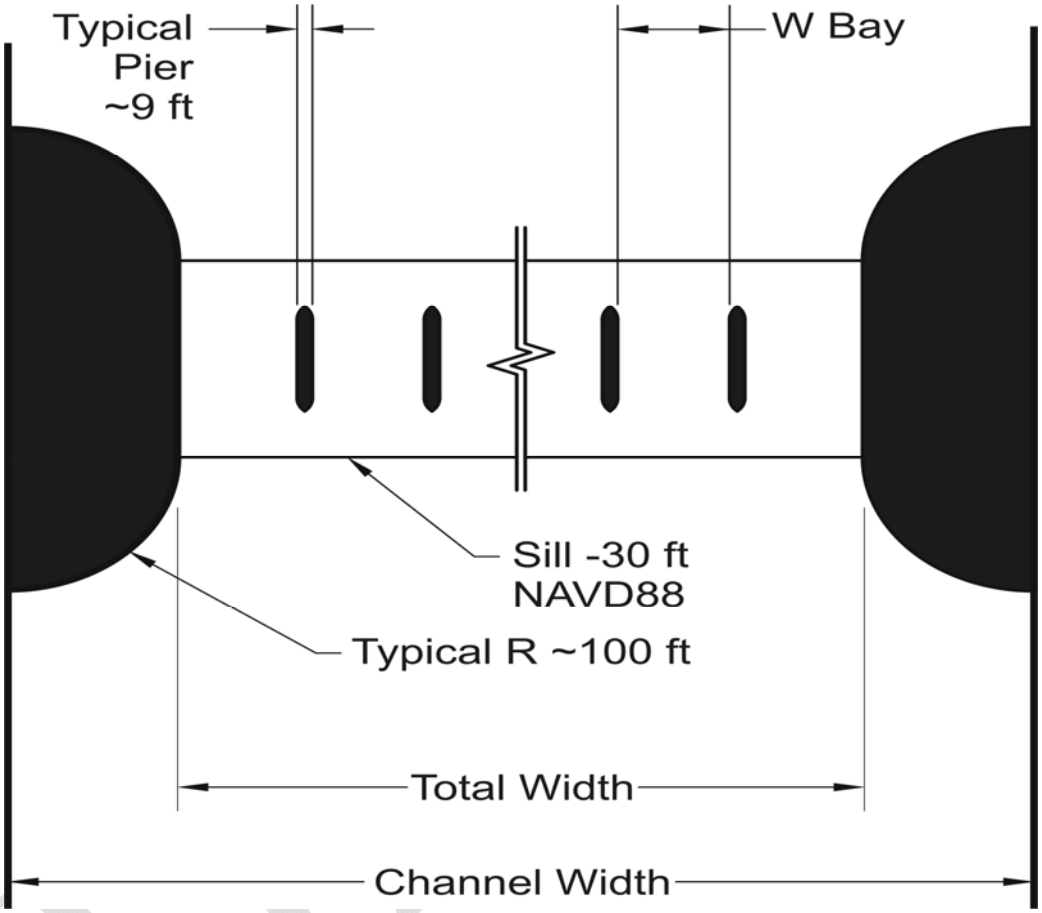

Figure 40 Plan View of Generic Flood Structure

Table 13 Structure Dimensions derived from Model Study

	Rigolets	**Chef**
W pier ft	9	9
W clear ft	1700	700
W bay ft	60	60
N bays	28	11
W total ft	1950	790
Sill ft NADV88	-30	-30

References

Blumberg, A. F., and Mellor, G. L., 1987, A description of a three-dimensional coastal model. Three Dimensional Coastal Ocean Models, N. S. Heaps, ed., American Geophysical Union, Washington, D.C., 1-16

Blumberg, A.F., Z-G Ji, and C.K. Ziegler., 1996, Modeling outfall plume behavior using far field circulation model. Journal of Hydraulic Engineering. Vol. 122, No. 11

Burchard, H., 2002. Applied turbulence modeling in marine waters. Springer:Berlin-Heidelberg-New York-Barcelona-Hong Kong-London-Milan Paris-Tokyo, 215pp.

Chen, C., Beardsley, R., Cowles, G., 2006. An Unstructured Grid, Finite-Volume Coastal Ocean Model, FVCOM User Manual, SMAST/UMASSD-06-0602, 315 pp.

Chen, C., Liu, H., Beardsley, R., 2003. An Unstructured Grid, Finite-Volume, Three-Dimensional, Primitive Equations Ocean Model: Application to Coastal Ocean and Estuaries, Journal of Atmospheric and Oceanic Technology, America Meteorological Society, Vol. 20, 159 – 186.

Civil and Environmental Engineering Department, University of New Orleans, Sogreah Ingenierie and Coastal Restoration Consultants. 1997. The Transportation of Sediment by Gravity for Coastal Restoration and Wetland Rehabilitation in Louisiana, Feasibility Study and Report for the Department of Natural Resources, State of Louisiana.

Georgiou, I. Y., 2002. Three-dimensional hydrodynamic modeling of salinity intrusion and circulation in Lake Pontchartrain, Ph.D. Dissertation, Dept. of Civil and Environmental Engineering, University of New Orleans, New Orleans, LA, 171 pp.

Haralampides, K., 2000. A study of the hydrodynamics and salinity regimes of the Lake Pontchartrain system, Ph.D. Dissertation, Dept. of Civil and Environmental Engineering, University of New Orleans, New Orleans, LA, 219 pp.

HydroQual, Inc., 2002, A primer for ECOMSED. Users Manual, Ver. 1.3, HydroQual, Inc., Mahwah, NJ, USA, 188pp.

Mellor, G.L. and Yamada, T., 1982, Development of a turbulence closure model for geo-physical fluid problems. Reviews of Geophysics and Space Physics, 20, 851-875

Oey, L.-Y., G. L. Mellor, and R. I. Hires., 1985b, A three-dimensional simulation of the Hudson-Raritan estuary. Part II: Comparison with observation, J. Phys. Oceanogr., 15, 1693-1709

Oey, L.-Y., G.L. Mellor, and R. I. Hires., 1985a, A three-dimensional simulation of the Hudson-Raritan estuary. Part I: Description of the model and model simulations, J. Phys. Oceanogr, 15, 1676-1692.

Reid, R.O., Bodine, B. R., 1968, Numerical Model for Storm Surges in Galveston Bay. ASCE Journal of Waterways and Harbors Division, Vol. 94, No. WW1

Shulman, I., and J.K. Lewis, 1995, Optimization approach to the treatment of open boundary conditions. J. Phys. Oceanogr., 25, 1006-1011

Smolarkiewicz, P.K., 1984, A fully Multidimensional Positive Definite Advection Transport Algorithm with Small Implicit Diffusion. J. Comp. Phys., 54:325-362

U. S. Army Corps of Engineers, 1984, Mississippi and Louisiana Estuarine areas: Freshwater Diversion to Lake Pontchartrain Basin and Mississippi Sound- Feasibility Study- New Orleans District

Appendix A

USGS monitoring data at Pass Rigolets near Lake Borgne

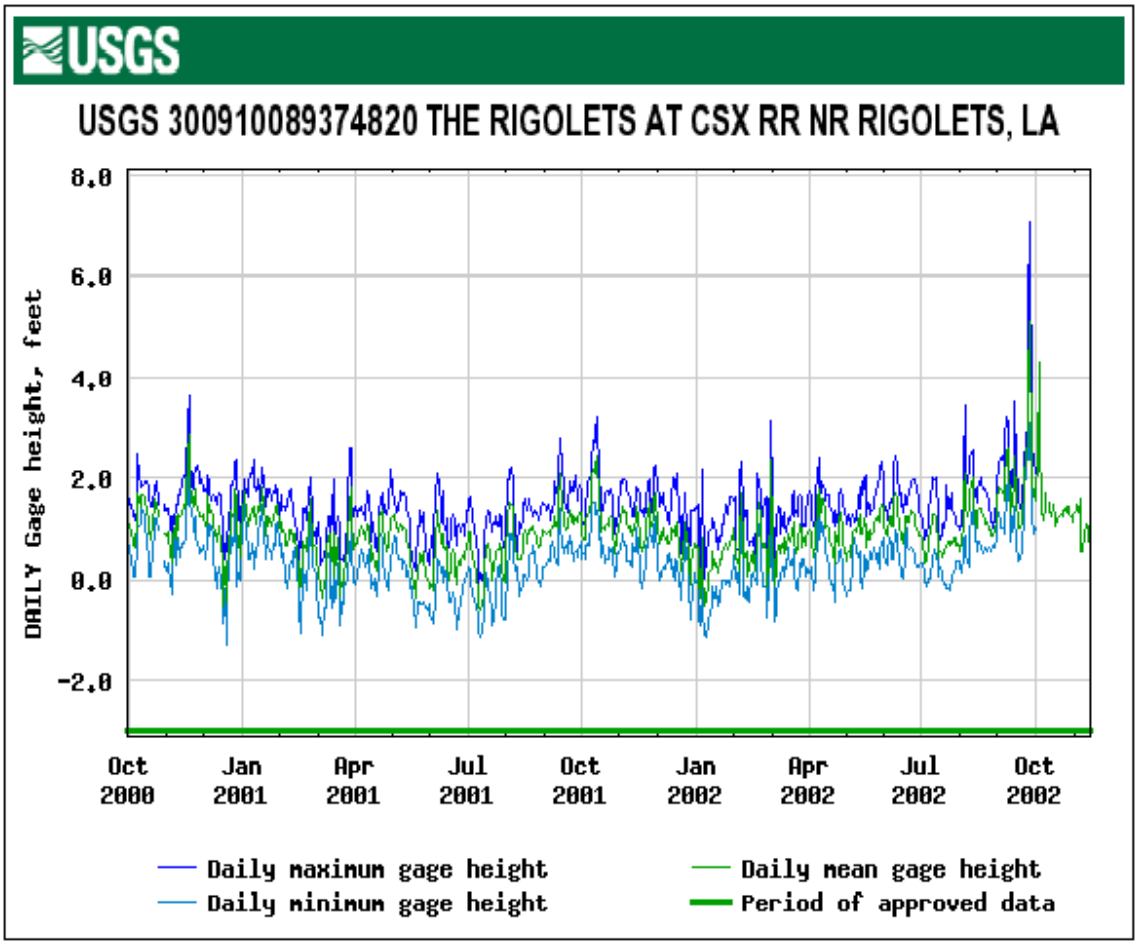

Figure A1. Variation in Stage at Lake Borgne End of the Rigolets Pass (from USGS)

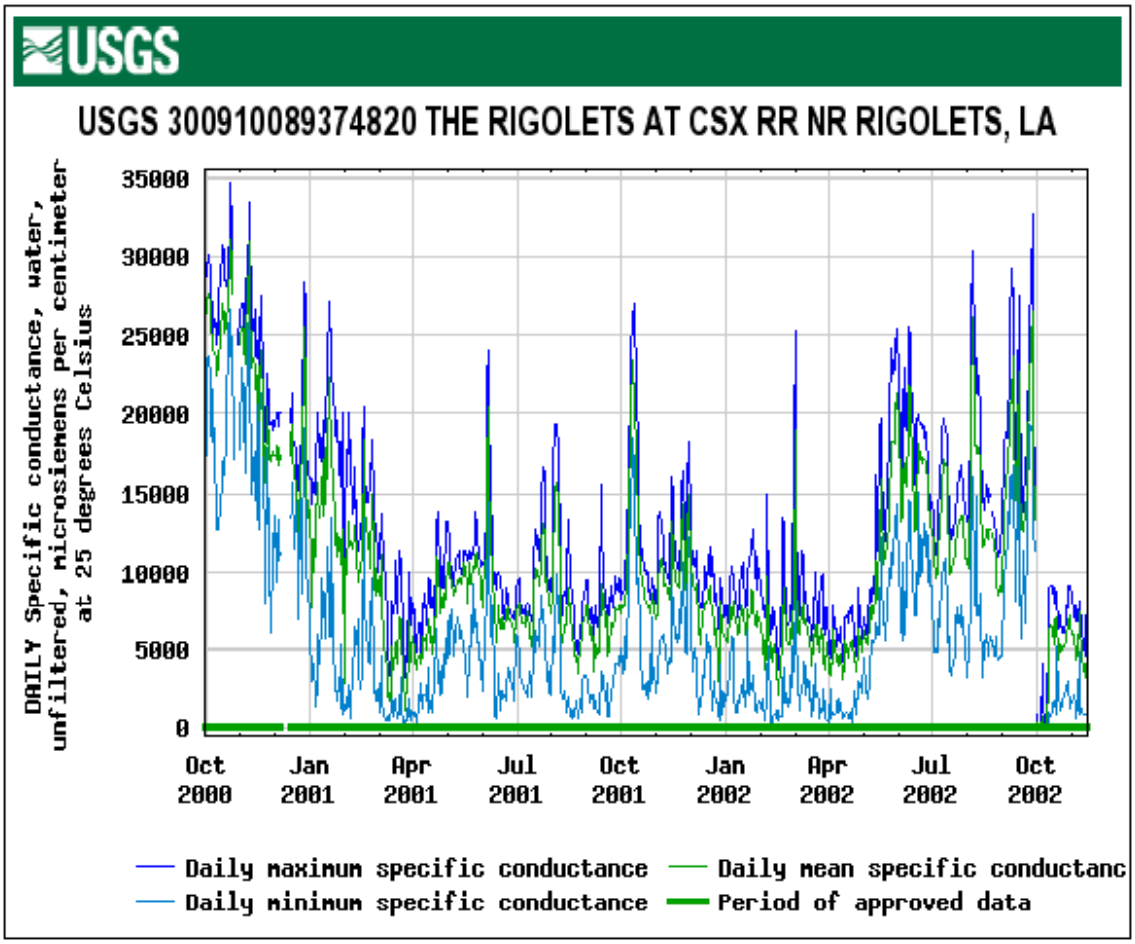

Figure A2. Variation in Specific Conductance at Lake Borgne End of Rigolets Pass (from USGS)

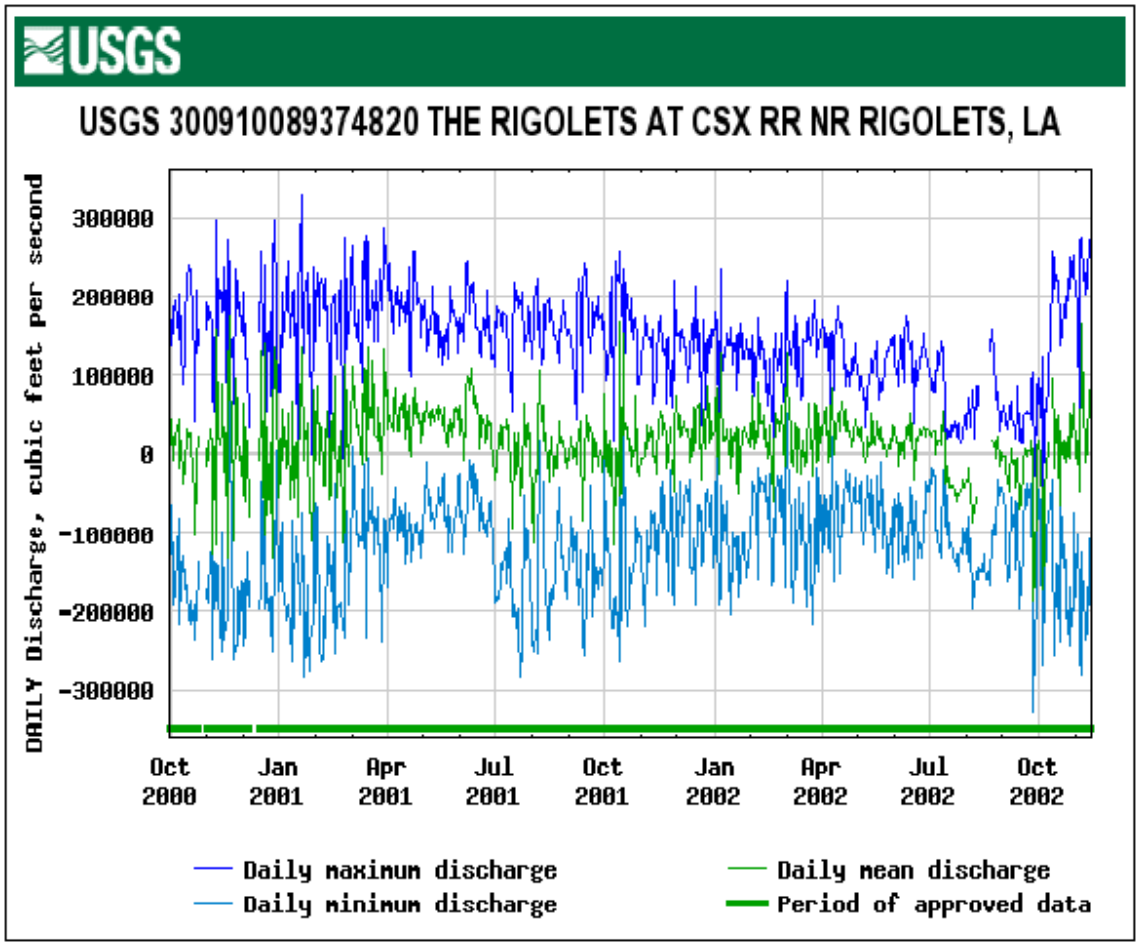

Figure A3. Variation in Discharge at Lake Borgne End of Rigolets Pass. (from USGS)

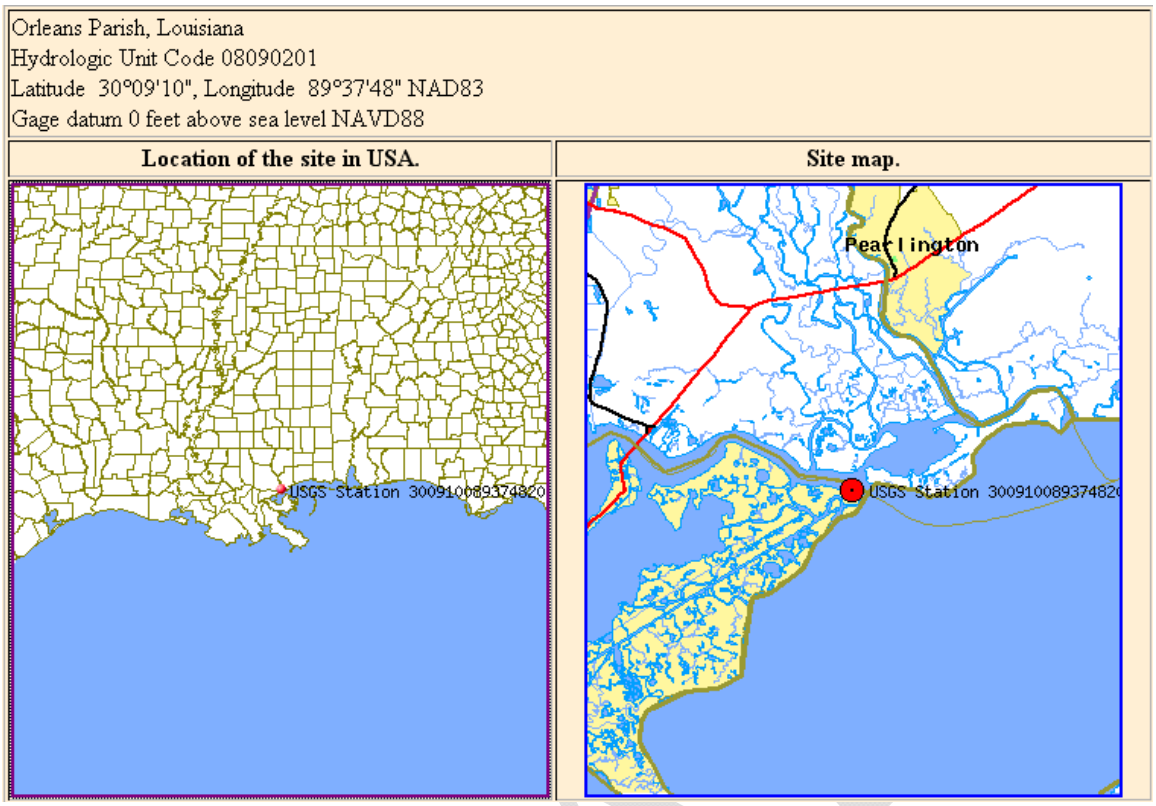

Figure A4. Location of USGS Station at Lake Borgne End of Rigolets Pass

Appendix B

Table B1. Comparison of Existing Lake Pontchartrain Tidal Prism with Structural Option 6b (1700 ft clear width at the Rigolet and 700 ft at the Chef)

Location	RMS deviation [m]	Average [m]
West Rigolets base	0.101	
West Rigolets For Structures	0.098	
% Difference	*-3%*	
West Chef base	0.088	
West Chef For Structures	0.086	
% Difference	*-1%*	
Midlake base	0.046	
Midlake For Structures	0.042	
% Difference	*-7%*	
LUMCON base	0.046	
LUMCON For Structures	0.043	
% Difference	*-8%*	
Average of base	0.047	0.063
Average for Structure cases	0.044	0.065
Percentage difference	-5%	2%
	Depth[ft]	Width [ft]
Rigolets	30	1950 (1700 ft clear)
Chef	30	840 (700 ft clear)

TableB2. Statistical Parameters (Comparison between the shallow draft structure on the navigation complex and base case with normal tides)

Location	RMS deviation	Average, m
West Rigolets base	0.102	
West Rigolets shallow draft	0.105	
% Difference	*3%*	
West Chef base	0.089	
West Chef shallow draft	0.091	
% Difference	*2%*	
Midlake base	0.046	
Midlake shallow draft	0.044	
% Difference	*-5%*	
LUMCON base	0.047	
LUMCON shallow draft	0.044	
% Difference	*-5%*	
Lake Average of base	0.063	0.05
Lake Average of shallow draft cases	0.061	0.05
		<1% relative to maximum tidal range in Lake
Percentage difference	-3%	Pontchartrain
	Depth[ft]	Width [ft]
Rigolets	Existing	Existing
Chef	Existing	Existing

Table B3. Statistical Parameters: Comparison between base case and structures case with normal tides and the Bonnet Carré. (8b versus Bonnet Carré base)

Location	**RMS deviation [m]**	**Average, m**
West Rigolets base	0.129	
West Rigolets For Structures	0.123	
% Difference	*7%*	
West Chef base	0.125	
West Chef For Structures	0.120	
% Difference	*9%*	
Midlake base	0.135	
Midlake For Structures	0.129	
% Difference	*10%*	
LUMCON base	0.134	
LUMCON For Structures	0.128	
% Difference	*9%*	
Average of base	0.132	0.288
Average of Structures case	0.126	0.289
Percentage difference	<5%	<+1%
	Depth[ft]	Width [ft]
Rigolets	30	1950 (1700 ft clear)
Chef	30	840 (700 ft clear)

Table B4. Statistical Parameters (Comparison between base case and structures case with extratropical tides) 9a versus 4

Location	RMS deviation [m]	Average, m
West Rigolets base	0.294	
West Rigolets For Structures	0.286	
% Difference	*-3%*	
West Chef base	0.291	
West Chef For Structures	0.286	
% Difference	*-2%*	
Midlake base	0.290	
Midlake For Structures	0.290	
% Difference	*0%*	
LUMCON base	0.291	
LUMCON strcr	0.290	
% Difference	*0%*	
Average of base	0.218	0.46
Average of Structures case	0.216	0.46
Percentage difference	<-1%	<1%
	Depth[ft]	Width [ft]
Rigolets	30	1950 (1700 ft clear)
Chef	30	840 (700 ft clear)

Table B5. Statistical Parameters (Comparison between base case and structures case with extratropical tides and Bonne Carré) 9b vs 3

Location	RMS deviation [m]	Average, m
West Rigolets base	0.33	
West Rigolets For Structures	0.33	
% Difference	*0%*	
West Chef base	0.33	
West Chef For Structures	0.33	
% Difference	*-0%*	
Midlake base	0.36	
Midlake For Structures	0.36	
% Difference	*-1%*	
LUMCON base	0.36	
LUMCON For Structure	0.36	
% Difference	*-1%*	
Average of base	0.35	0.56
Average of Structures case	0.35	0.56
Percentage difference	<-1%	<1%
	Depth[ft]	Width [ft]
Rigolets	30	1950 (1700 ft clear)
Chef	30	840 (700 ft clear)

Appendix C

Figure C1 shows the water elevations, Surface velocities and energy grade line through an 800 ft structure in the Rigolets with a typical spring tide and receding storm surge from Lake Pontchartrain. The ECOMSED model indicated an excessive high velocity zone (> 3 m/s) that extended several channel widths from the structure. On either side of this high velocity zone there are elongated eddies with velocities that exceed 1.5 m/s. Figures C2 to C4 indicate the progressive improvement for openings of 1500, 1700 and 1975 ft respectively. The drop in total energy across the structure is close to 1 m for an 800 ft wide structure and 0.02 m for a 1975 ft structure.

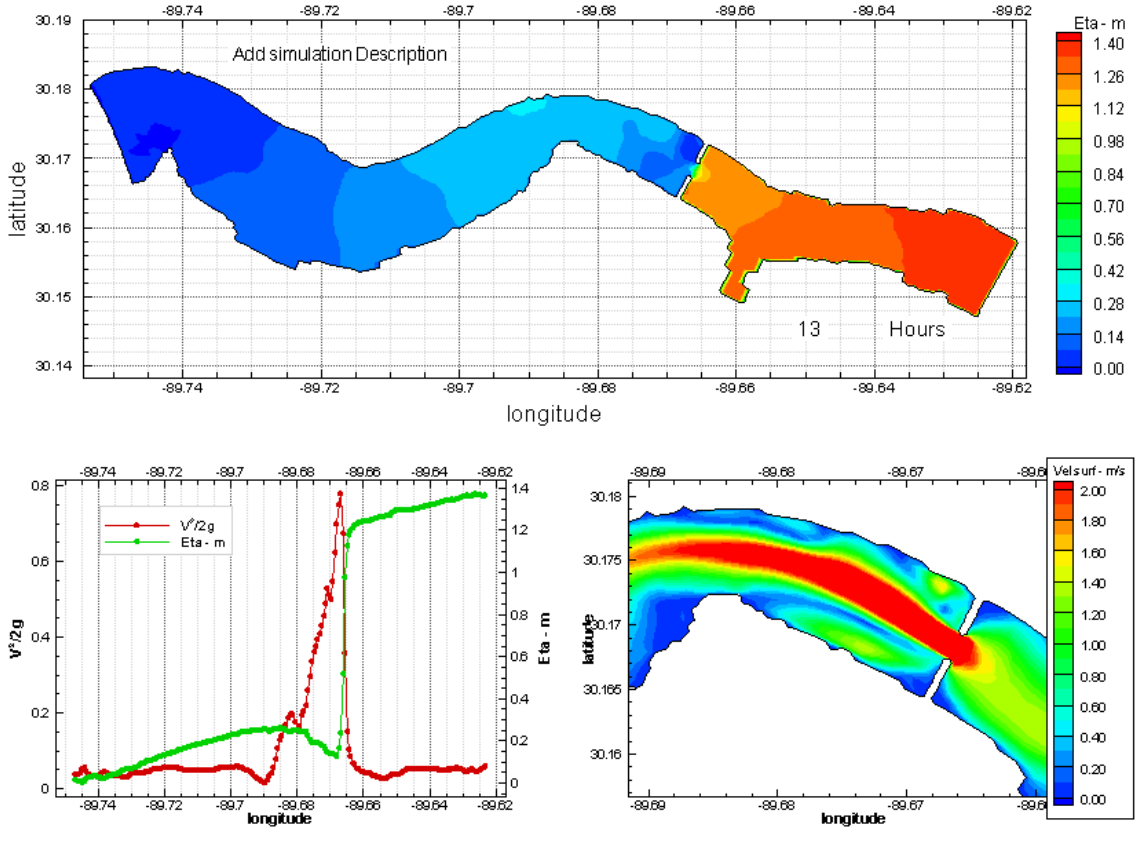

Figure C1. Distribution of free surface elevation, velocity head, differential head loss and surface velocity for a 800 ft structure during flood; Storm flow of 290,000 cfs.

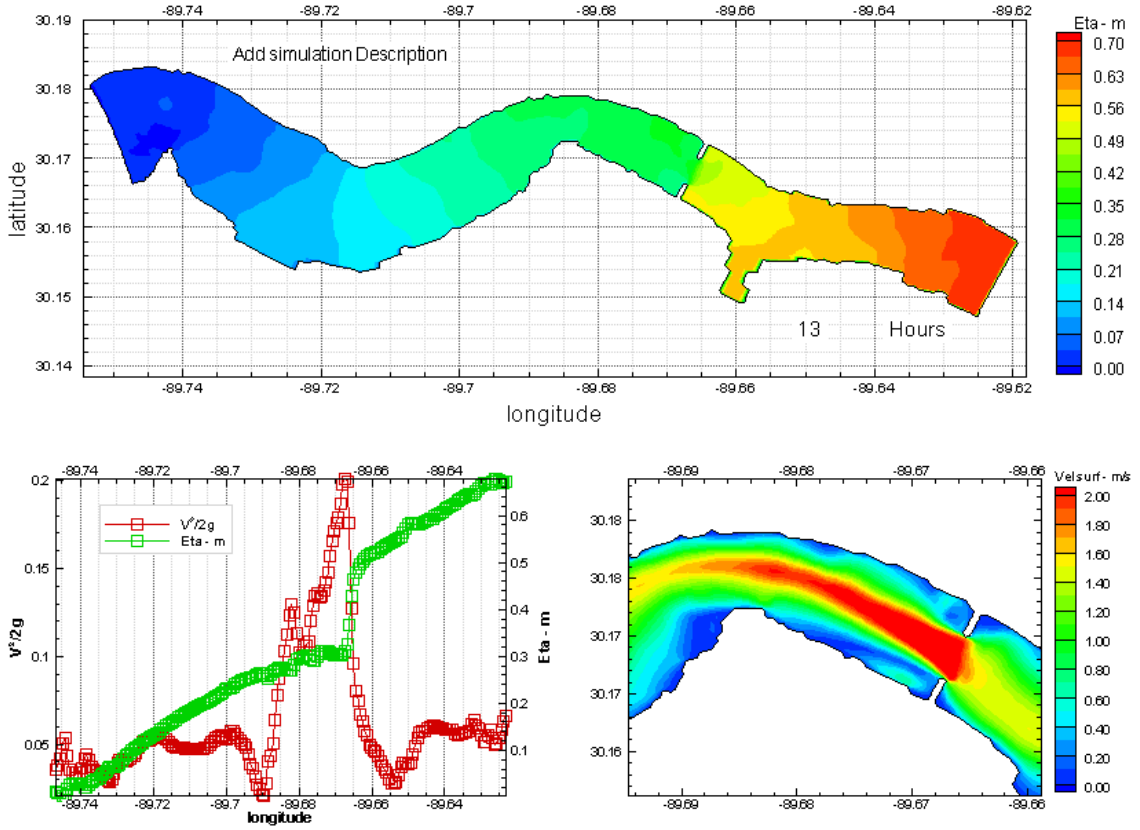

Figure C2. Distribution of free surface elevation, velocity head, differential head loss and surface velocity for a 1500 ft structure during flood; Storm flow of 290,000 cfs.

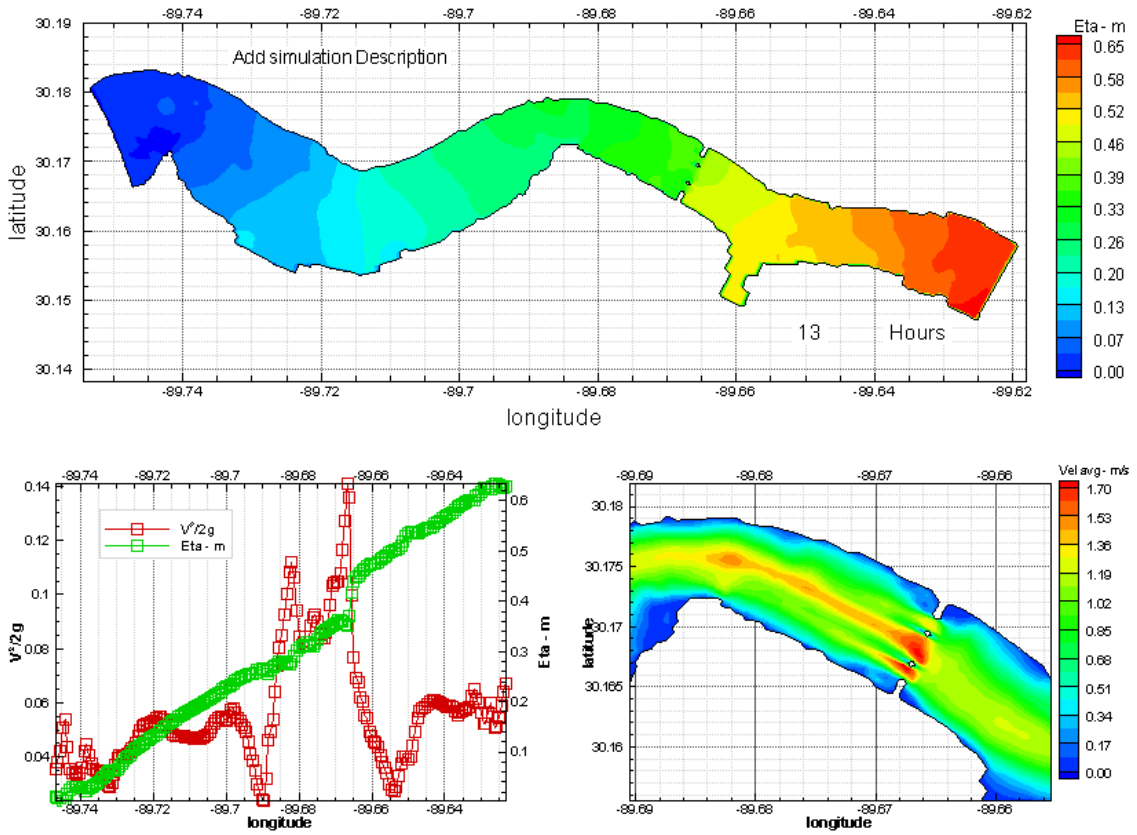

Figure C3. Distribution of free surface elevation, velocity head, differential head loss and surface velocity for a 1700 ft structure during flood; Storm flow of 290,000 cfs.

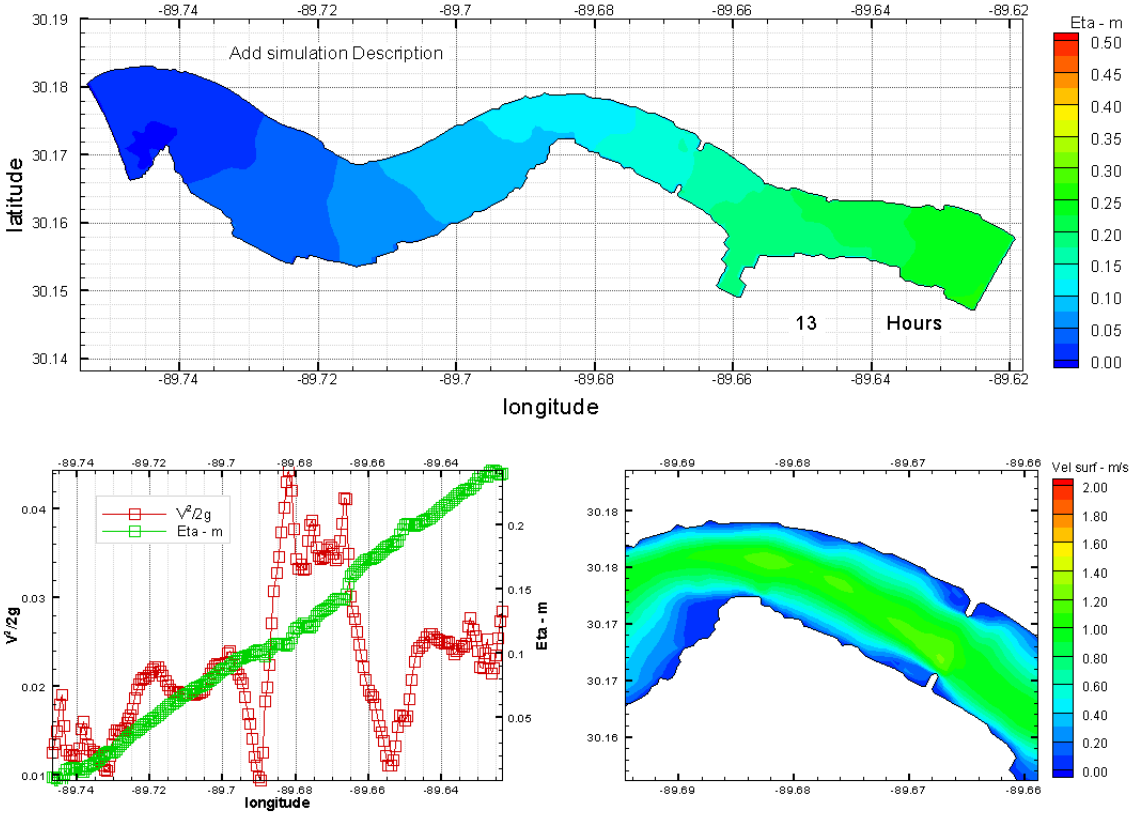

Figure C4. Distribution of free surface elevation, velocity head, differential head loss and surface velocity for a 1975 ft structure during flood; Normal flow of 185,000 cfs.